Title: CDK12 inhibition reduces abnormalities in cells from patients with myotonic dystrophy and in a mouse model *

Authors: Ami Ketley[1], Marzena Wojciechowska[1], Sonja Ghidelli-Disse[2], Paul Bamborough[3], Tushar K Ghosh[1], Marta Lopez Morato[1], Saam Sedehizadeh[1], Naveed Altaf Malik[1], Zhenzhi Tang[4], Paulina Powalowska[1, 5], Matthew Tanner[4], Rudolf Billeter-Clark[1], Rebecca C Trueman[1], Philippine C Geiszler[1], Alessandra Agostini[1], Othman Othman[1], Markus Bösche[2], Marcus Bantscheff[2], Martin Rüdiger[6], Danuta E Mossakowska[7,8], David H Drewry[9], William J Zuercher[9,10], Charles A Thornton[4], Gerard Drewes[2], Iain Uings[7], Christopher J Hayes[5], J David Brook[1*].

Affiliations:

[1] School of Life Sciences, University of Nottingham, Queen's Medical Centre, Nottingham, NG7 2UH, United Kingdom

[2] Cellzome GmbH, Molecular Discovery Research, GlaxoSmithKline, Meyerhofstrasse 1, 61997, Heidelberg, Germany

[3] Computational and Modelling Sciences, GlaxoSmithKline, Medicines Research Centre, Hertfordshire, SG1 2NY, United Kingdom

[4] Department of Neurology, University of Rochester Medical Center, Rochester, New York, 14642-0001, United States of America

[5] School of Chemistry, University of Nottingham, University Park, Nottingham, NG7 2RD, United Kingdom

[6] Screening Profiling and Mechanistic Biology, GlaxoSmithKline, Medicines Research Centre, Hertfordshire, SG1 2NY, United Kingdom

[7] Discovery Partnerships with Academia, GlaxoSmithKline, Medicines Research Centre, Hertfordshire, SG1 2NY, United Kingdom

[8] Malopolska Centre of Biotechnology, Jagiellonian University, 30-348, Krakow, Poland

[9] Department of Chemical Biology, GlaxoSmithKline, Research Triangle Park, North Carolina, 27709-3398, United States of America

[10] SGC Center for Chemical Biology, UNC, Eshelman School of Pharmacy, NC 27599, United States of America

*Corresponding author: David Brook. Email: david.brook@nottingham.ac.uk

Abstract: Myotonic Dystrophy type 1 (DM1) is an RNA-based disease with no current treatment. It is caused by a transcribed CTG-repeat expansion within the 3' untranslated region (UTR) of the dystrophia myotonica protein kinase (*DMPK*) gene. Mutant repeat expansion transcripts remain in the nuclei of patients' cells, forming distinct microscopically detectable foci that contribute substantially to the pathophysiology of the condition. Here we report small molecule inhibitors that remove nuclear foci and have beneficial effects in the HSA^{LR} mouse model, reducing transgene expression leading to improvements in myotonia, splicing and centralized nuclei. Using chemoproteomics in combination with cell-based assays, we identify cyclin-dependent kinase 12 (CDK12) as a druggable target for this condition. CDK12 is a protein elevated in DM1 cell lines and patient muscle biopsies and our results showed that its inhibition led to reduced expression of repeat expansion RNA. Some of the inhibitors identified in this study are currently the subject of clinical trials for other indications and provide valuable starting points for a drug development program in DM1.

One sentence summary: CDK12 inhibition reduces mutant transcripts and nuclear foci in DM1 cells and produces splicing correction and phenotypic benefit in a mouse model.

Introduction

Myotonic Dystrophy type 1 (DM1) is the most common form of adult muscular dystrophy which affects 1 in 8,000 people (*1*). It is caused by a CTG repeat sequence in the 3' untranslated region of the *DMPK* gene (*2-4*), which is greatly expanded in patients who may have 50 to several thousand repeats on affected chromosomes compared to between 5 and 37 repeats on unaffected chromosomes. The expanded repeat is transcribed, and despite being correctly spliced, the repeat expansion transcripts remain sequestered in the nucleus forming distinct foci (*5-7*). These foci interact with cellular proteins, such as muscleblind-like splicing regulator 1 (MBNL1), a key

splicing regulator, which in turn leads to downstream splicing abnormalities (*8, 9*). In addition to the sequestration of proteins, the mutant RNA causes activation of CUGBP, Elav-like family member 1 (CELF1), which is also implicated in splicing (*10*). Additional molecular pathways are thought to be affected by the toxic RNA, including repeat associated non-AUG (RAN) translation and inhibition of translation (*11, 12*).

There is currently no treatment for DM1, and disease management relies on a fragmented approach utilizing specific drugs for the piecemeal treatment of particular symptoms such as mexiletine to treat myotonia and modafinil to address daytime sleepiness (*13, 14*). However, due to the complex and variable nature of DM1, management of individual symptoms is not an efficient way to manage the condition and an effective treatment is required. Drug development for an RNA-based disorder such as DM1 represents a major challenge due to the lack of a suitable protein target (*15-21*). Previously we reported an optimized high content screening assay to test the effect of small molecules on nuclear foci in DM1 and identified the possible role of a kinase as central to disease pathophysiology (*22*). Thus, we set out to identify the specific kinase involved in reducing the accumulation of CUG nuclear foci as a cellular target for DM1 therapy.

Results

Identification of compounds that reduce nuclear foci

Our previous work indicated the involvement of kinases in DM1 pathophysiology, and the use of kinase inhibitors reduced nuclear foci leading to downstream beneficial cellular effects (*22*). To identify the specific kinase target we utilized the GlaxoSmithKline Published Kinase Inhibitor Set (PKIS) (*23*). Using our previously reported assay we screened the PKIS collection for compounds able to reduce nuclear foci. This assay used high content imaging to identify the nuclear compartment and quantify foci within this region. Foci were defined based on fluorescent intensity above background and at least 300 cells were imaged for each compound concentration (*22*). Six compounds that share a pyrazolo[1,5b]pyridazine core were found to reduce the number of nuclear foci following 24-hour treatment of DM1 cells (Fig. 1A-F, fig. S1). This result was consistent across 2 DM1 fibroblast lines (table S1). We then analyzed the known selectivity profiles of these six compounds to identify the common kinase targets. The log half maximal inhibitory concentration (pIC_{50}) values generated from the foci assays were compared to the compound inhibition profiles against 224 kinase targets (*23*). A partial least squares (PLS) model was used to cluster the data, which suggested that the common target was likely to be a member of the cyclin-dependent kinases (CDKs), mitogen-activated protein kinases (MAP kinases), glycogen synthase kinases (GSKs) and CDK-like kinases (CMGC) family (Fig. 1G). The CMGC family members were then further analyzed to identify the most likely target candidates within this group (fig. S2). We compared the kinase percentage inhibition value for all tested compounds, categorizing the six nuclear foci reducing compounds as active and the remaining compounds that did not result in nuclear foci reduction as inactive (fig. S2). The resulting scatterplots were then evaluated to identify if any of the kinase targets showed a clear difference in activity between the actives and

the inactives. Of the targets covered by the PKIS collection, CDK family members appeared most likely to be involved, specifically CDK4, which showed that the six nuclear foci reducing compounds had higher inhibitory activity on this target than all other compounds tested (fig. S2D). To evaluate the potential role of CDK family members on nuclear foci modulation, we tested additional small molecule CDK inhibitors with well-annotated selectivity profiles (fig. S1, fig. S3, table S2) in the nuclear foci assay. CDK family inhibitors dinaciclib and SNS-032 reduced nuclear foci (Fig. 1H-I), further suggesting that CDKs could play a role in the pathophysiology of DM1.

Inhibitor treatment as a therapeutic for DM1

Both dinaciclib and SNS-032 have been used in early clinical trials for cancer therapy (*24-28*). To investigate the potential use of such compounds as a therapy in DM1 we sought to establish the time-course of inhibition on nuclear foci and to determine the minimal exposure time required for beneficial effect. To determine a dosing regimen with these inhibitors we exposed DM1 fibroblasts to SNS-032 for 2 hours, after which time the cells were washed thoroughly and allowed to recover in complete growth media. Quantification of untreated DM1 cells showed that 68% had 5 or more foci/cell and only 5% had no detectable foci (Fig. 2A). When cells were treated with SNS-032 for 2 hours, with no recovery time, this distribution shifted to 28% of cells with 5 or more foci and 10% cells with no foci (Fig. 2B). With increased recovery times of 48 and 72 hours, the proportion of cells without nuclear foci increased further to 14% and 36%, respectively (Fig. 2C-D). A short (2 hour) treatment with inhibitor, followed by a prolonged (72 hour) recovery, led to a significant reduction in nuclear foci (Chi squared test: $p<0.0001$ for all dosing regimen compared to untreated cells), suggesting that pulsatile treatment could be an efficacious approach to DM1 therapy with suitable inhibitors.

Nuclear foci are a key cellular feature in DM1 and act as a useful biomarker for screening. Ultimately, we wanted to understand the effect of compounds on the repeat expansion transcript directly and to assess any downstream effects. Therefore, we next sought to establish the effect of inhibitor treatment on *DMPK* transcripts. Following treatment with dinaciclib, we utilized a previously reported assay based on the presence or absence of a coding *Bpm*I polymorphism (SNP rs527221) that allows us to distinguish between wild-type and mutant *DMPK* transcripts in informative patient cell lines (*7*). Analysis of nuclear and cytoplasmic cell extracts showed that the repeat expansion transcripts were still retained within the nuclear fraction (Fig. 2E). However, quantification using Genescan analysis showed a 59% decrease in the relative proportion of repeat expansion transcripts compared to unexpanded *DMPK* transcripts in the nucleus following inhibitor treatment (2 way ANOVA, $p<0.0001$ (Fig. 2F)). To confirm this result, we employed digital droplet PCR (ddPCR) to quantify the wild type and mutant *DMPK* transcript numbers in total RNA from two DM1 fibroblast cell lines treated with our most potent compounds, SNS-032 and dinaciclib (Fig. 2G-2J, fig. S4). Treatment reduced nuclear foci and did not result in cellular toxicity. The data shows a reduction between 20 and 60% in mutant repeat-containing transcripts. Only in the HK DM1 fibroblast cell line treated with SNS-032 was a reduction seen in the wild type transcript (Fig. 2J). Thus, exposure to these CDK inhibitors appears to reduce predominantly the repeat-containing transcript.

To examine if this beneficial effect was translated into an in vivo model we treated human skeletal actin, long repeat) (HSA^{LR}) transgenic mice, a mouse model of DM1, with 20 mg/kg dinaciclib by intraperitoneal injection. The dosing regimen of dinaciclib was established based on previously

tested doses and tolerability studies in mice and human clinical cancer studies (*29*). The HSA^{LR} mice express repeat expansion RNA at amounts 5- to 8-fold higher than human DM1 muscle (*30*). Blinded analysis was performed 1 day after the final injection. Mice were age and sex matched to assess the effect on nuclear foci, HSA transgene amounts and key splice isoform profiles in vehicle and dinaciclib-treated samples. Following dinaciclib treatment we observed a reduction in the number of cells containing nuclear foci (Fig 3A and B). Likewise when we quantified the repeat containing transcript directly by ddPCR we found a significant reduction in the relative amounts of the HSA transgene in dinaciclib treated animals (Fig. 3C, t-test $p<0.0001$). This is consistent with the data observed in DM1 fibroblast lines. To assess any beneficial effect on mis-splicing we studied 9 transcripts, known to be dysregulated in DM1 (*31-37*). Across the panel of genes we consistently observed improvements in dinaciclib-treated mice (Fig. 3D, fig. S5) Additionally we collected muscle samples from vehicle and dinaciclib-treated mice. Staining of muscle fibers highlighted a reduction in the presence of centralized nuclei within muscle fibers following inhibitor treatment (fig. S6A-B, t-test; $p=0.0162$). To understand if the observed molecular changes resulted in any functional improvement we conducted electromyography (EMG) and graded the animals with a myotonia grade from 0-3, with 3 being the most severe. Dinaciclib treatment improved myotonia in all muscles analyzed except the tibialis anterior (Fig. 3E, Mann-Whitney; $p=0.0443$, additional data: fig. S6C-D).

Kinase inhibitor target deconvolution

To identify the specific CDK target responsible for these beneficial effects we used the kinobeads methodology, which is based on sepharose beads derivatized with a combination of promiscuous

kinase inhibitors (*38-40*), to profile 11 compounds, which represent a range of activities in the nuclear foci assay. Target profiles were generated by adding each compound to K562 erythroleukemia cell extract at a concentration of 2μM, followed by incubation with two variations of kinobeads and quantification of bead-bound proteins (*38, 41*) . The profiling results suggested that members of the CDK family are common targets of the most active compounds (table s3), consistent with the PKIS data.

We sought to expand the target coverage within the CDK family by the immobilization on beads of two of the active compounds containing a suitable secondary amine; SNS-032 and AT7519 (fig. S7). Beads derivatized with either compound showed good coverage of the CDK family, including family members against which the PKIS collection was not profiled. For an in-depth chemoproteomics study, profiling inhibitor selectivity across the CDK family, we generated dose-response competition-binding profiles for all active and one of the inactive compounds (PD0332991) in K562 cells or in A204 rhabdomyosarcoma cells (dataset S1). We also conducted a comparative whole proteome analysis to confirm that the K562, A204 and DM1 cell lines express the same kinases (dataset S1, dataset S2). All CDK/PCTK proteins identified by profiling were also identified in the cells used for the nuclear foci assay (fig. S8, dataset S1, dataset S2). The resulting dataset comprises IC_{50} curves for 12 CDK family kinases (fig. S9, table S4). To identify the most likely kinase target we plotted pIC_{50} values for kinobead binding against the pIC_{50} in the foci inhibition assay for each compound. A good correlation of kinase binding affinity with the inhibitory activity on foci was observed for CDK7, CDK9, and CDK12. The best correlation of kinase pIC_{50} values with inhibitory activity on foci was observed for CDK12. Dinaciclib was the most potent inhibitor against the CDK family, in particular against CDK12 (Fig. 4).

CDK12 in DM1 pathogenesis

To examine the potential involvement of CDK12 in DM1 pathogenesis, we assessed the endogenous amounts of this protein in vastus lateralis muscle biopsy samples from four patients with DM1 and four healthy volunteers using western blot. (Fig. 5A). There was an increase in CDK12 in DM1 biopsies versus those from healthy volunteers, with 48% more CDK12 protein detected in DM1 samples (t-test $p=0.02$, Fig. 5B).

Next, we used immunohistochemistry to examine the location of CDK12 in DM1 fibroblasts. Consistent with previously published data from non-DM1 cells that shows CDK12 co-localization with SC35 speckles, we observed nuclear staining in granular structures in both DM1 and non-DM cells (*42*). Previous work has also identified a localization of CUG repeat expansion foci with nuclear speckles (*43*). Quantification of the CDK12 granular structures in 400 cells showed that the number of granules was significantly elevated in DM1 cells, with an average number of 18.74 (±3.88), compared to 12.07 (±2.27) in non-DM1 cells ($p<0.0001$, Fig. 5C). To understand further the relationship between CDK12 protein and repeat expansion foci and to confirm that specific inhibition of this protein was responsible for nuclear foci reduction, we used shRNA and siRNA to reduce CDK12 in DM1 cells. Following infection with lentiviruses (CrkRS shRNA (m) Lentiviral Particles, sc-44531-v) expressing three-five short hairpin RNAs (shRNAs) against CDK12 we observed a 56% reduction in the number of CDK12 granules and a 69% reduction in repeat expansion foci compared to scrambled shRNA treated cells (Fig. 5D-F, fig. S10). This was verified by siRNA knockdown of CDK12 and quantification by Western blot analysis (fig. S10). Conversely CDK12 overexpression with a full length open reading frame (ORF) clone resulted in

increased numbers of nuclear foci in a dose dependent manner (One way ANOVA p=0.0017, Fig. 5G).

CDK12 is a known regulator of transcription, specifically involved in transcriptional elongation, rather than at the initiation of transcription (*44*). To understand the mechanism by which CDK12 inhibition leads to nuclear foci reduction we tested the effect of CDK12 inhibition on repeat expansion transcription. For this we utilized a bi-directional inducible plasmid expressing eGFP in one direction and *DMPK* exons 10-15, containing 960 interrupted CTG repeats, in the other (*45*). This construct was transfected into mouse P19 cells in the presence or absence of the highly selective and potent CDK12 inhibitor, THZ531 (*46*) (Fig 5H, fig. S11). This compound was chosen for this analysis as, in contrast to dinaciclib, it is selective for CDK12 (*46*). Following doxycycline induction of the transgene, cells were harvested and RT-PCR and ddPCR analyses were conducted to establish the amounts of CUG 960 RNA and eGFP transcription. Transcript amounts were normalized to endogenous GAPDH. In untreated cells both transcripts accumulated at the same rate (fig. S12) whereas in THZ531-treated cells there was a clear reduction in the amount of CUG repeat expansion RNA following CDK12 inhibition compared to eGFP RNA (Fig. 5I, 5J). The amount of eGFP transcript did not show any differences in the presence or absence of CDK12 activity, suggesting that the inhibition of CDK12 leads to a preferential reduction in transcription of the expanded repeat (Fig 5I, 5J). To assess if CDK12 inhibition leads to increased rates of transcript decline we halted transcript production from the plasmid by removal of doxycycline and monitored the transcripts over 24 hours. This showed a natural reduction of both the CUG repeat expansion and eGFP transcripts at a similar rate (Fig. 5K, 5L and fig S12). The differential profiles for transcript accumulation suggest that the effect of CDK12 inhibition on the repeat expansion

transcript is specific at the level of transcript production, rather than a generalized effect on global transcription. To confirm this we conducted a nuclear run-on experiment to examine the transcription of wild-type and mutant transcript in untreated and THZ531-treated DM1 cells. This data supports the notion that in DM1 cells THZ531 inhibition affects transcription of the mutant transcript more than it affects the wild type transcript (t-test p=0.0017, Fig. 5M).

Discussion

The highly annotated PKIS collection provides an excellent resource for kinase inhibitor target deconvolution. We have employed this cheminformatic collection in conjunction with kinobead mass spectrometry to identify CDK12 as a cellular target for DM1 therapy. We utilized a phenotypic screen based on nuclear foci, a key molecular feature of this disease, as no clear molecular target was known and foci provide a visual biomarker of the condition. Our work has established a clear biological link between CDK12 and the molecular signature of DM1. CDK12 is a transcription elongation-associated C-terminal repeat domain (CTD) kinase, which has been shown to regulate phosphorylation of serine 2 in the C-terminal domain of RNA Pol II, a step required for productive elongation of transcripts, rather than being involved in the initiation of transcription (*44, 47*). The *S. cerevisiae* gene *CTK1*, an orthologue of metazoan CDK12, is not an essential gene and reports suggest CDK12 is not part of the core transcriptional apparatus (*42, 48*). Assessment of cell essentiality in human cell lines showed that CDK12 is essential in only one (KBM7 haploid cells) out of the 4 cell lines tested (KBM7, K562, Rao and Jiyoye) (*49*). Expression analysis showed that only 2.67% of genes, producing primarily long and complex transcripts, had altered amounts following CDK12 depletion, thereby providing a potential link between CDK12 and transcription of the DM1 expanded repeats (*50*). As CDK12 is not required at the start of

transcription and its inhibition does not result in global transcriptional arrest, alongside our data that shows continuous treatment is not necessary for beneficial effects, it may be suitable as a target for long term DM1 treatment.

Our results show that genetic knockdown of CDK12, or treatment with inhibitor, leads to reduced numbers of nuclear foci, which could be due to two possible mechanisms: reduced production of the mutant transcripts or their increased degradation. Using digital droplet PCR we show that selective inhibition of CDK12 results in a reduction in mutant RNA transcription, which points to a requirement for CDK12 to produce repeat expansion transcripts. Other than RNA Pol II, the targets of CDK12 phosphorylation are largely unknown, particularly in muscle, although it has been shown to suppress genes involved in supporting metabolic functions during stress and Reactive Oxygen Species (ROS)- induced gene activation (*51*).

Here we identify CDK12 as a druggable target for DM1. The development of specific CDK12 inhibitor molecules has been achieved and some of the molecules presented here have been the subject of clinical trials in other indications (*24-28*). Our data suggests that a pulsatile treatment resulting in a temporary transcriptional block in both cell lines and in vivo leads to beneficial downstream effects reducing nuclear foci, improving key splicing profiles and functional improvements in myotonia. The functional benefit observed in the HSA^{LR} mouse model demonstrates that the effects of CDK12 inhibition translate from cell-based assays to an in vivo model and provide evidence for the application of CDK12 inhibitors in DM1 therapy.

Further development of more selective CDK12 inhibitors will be required to fully understand the functional benefit of inhibiting this target for DM1 therapy. Furthermore the HSA^{LR} mouse does have limitations, despite being the best studied DM1 model, in that expression of the repeat

expansion transcript is driven from the skeletal actin promoter so these mice do not recapitulate all features of the disorder. The model has a repeat number of 250 CTG repeats, which is limited in size compared to what is seen in DM1 patients. Testing the effect of small molecules on other models should help understand the efficacy of CDK12 inhibition in the brain, for example. Future work will be required to refine the targeting of this protein in DM1, and the compounds presented here will act as valuable starting points and tool compounds for future drug development opportunities.

Materials and Methods

Study Design

The objective of this study was to identify the specific protein kinase responsible for previously observed beneficial effects in DM1 cell lines treated with kinase inhibitors. The design of the study was based on comparative analysis of compound activities in a cell-based screening assay with biochemical activity in in vitro assays. The PKIS collection was screened and the target refined using kinobead mass spectrometry. Following target identification, we tested key compounds in a DM1 in vivo model to establish the translational benefit of this kinase on key molecular events, transgene amounts and mis-spliced transcripts, and a key physiological output, myotonia.

All cell-based screening assays were unblinded but performed in triplicate with appropriate controls and analyzed with an automated process. For in vivo experiments, mice were randomized to treatment groups and all tests were carried out and analyzed in a blinded manner. Power calculations established treatment groups for EMG of 9 mice per group. (Gpower v3.1, for a Wilcoxon-Mann-Whitney test for a 50% reduction in scores, based on variance from (*52*) Alpha = 0.05, power = 0.90, d=1.5). All experiments were carried out in three biological replicates, unless stated otherwise in the figure legend. Experimental details and the statistical tests used are listed in each figure legend. All data are presented and includes all outliers. Raw data and the corresponding statistical test details for the figures are listed in Supplementary data file S3.

Sample Use

The human biological samples were sourced ethically and their research use in accord with the terms of the informed consent. All animal studies were ethically reviewed and carried out in accordance with Animals (Scientific Procedures) Act 1986 and the GSK Policy on the Care, Welfare and Treatment of Animals. All experiments were performed in accordance with relevant guidelines and regulations of the Animal Procedures Act under license number PPL3003449 (Nottingham), issued 2016-12-05, and granted by The Home Office. All studies were reviewed and conducted in accordance with the Institutional Animal Care and Use Committee by the ethical review process at the institution where the work was performed.

Cell Culture

Fibroblast cells were grown in Dulbecco's Modified Eagles Medium (DMEM) with penicillin and streptomycin, and 10% fetal calf serum (FCS) (Sigma). KB Telo MyoD cell line contains 400 CTG repeats, LR Telo MyoD cell line contains 1200 CTG repeats, HK Telo MyoD cell line contains 1600 CTG repeats.

***In situ* hybridization protocol**

Cells were exposed to compounds for 24hrs after which in situ hybridization was performed to identify foci using a Cy3 labelled $(CAG)_{10}$ probe. Plates were analyzed on a Molecular Devices Micro High Content Imaging system, with nine fields imaged per well to give approximately 100 cells per well, per compound treatment. The nuclear area was identified by Hoechst stain and the number, size and intensity of foci were determined by scoring adjacent pixels that were 80 grayscales or more above background.

Preparation of cell extracts

K562 and A204 cells were obtained from the American Type Culture Collection (ATCC) and cultured in Roswell Park Memorial Institute (RPMI) medium containing 10% FCS. Cells were expanded to 1.5×10^6 cells/ml. A204 cells were cultured in McCoy´s 5A medium containing 15% FCS. Cells were expanded to 100% confluency. Cells were harvested and subjected to 3 washes with ice-cold phosphate buffered saline (PBS). Aliquots were snap frozen in liquid nitrogen and stored at −80 °C. Cell extracts were prepared as described (*53*).

Chemoproteomics

Affinity profiling was performed as described previously (*38, 53*). Sepharose beads were derivatized with SNS-032 or AT7519 at a concentration of 1 mM to generate a bead matrix, or Kinobeads were used as a matrix for profiling. Beads (35 µl in case of Kinobeads or 5 µl in case of SNS-032) were washed and equilibrated in lysis buffer at 4 °C for 1 h with 1 ml (5 mg) K562 cell extract, which was pre-incubated with compound or buffer. Beads were transferred to disposable columns (MoBiTec), washed extensively with lysis buffer and eluted with sodium dodecyl sulphate (SDS) sample buffer. Proteins were alkylated, separated on 4–12 % NuPAGE (Invitrogen), stained with colloidal Coomassie, and quantified by isobaric mass tagging and liquid chromatography tandem mass spectrometry (LC-MS/MS).

ddPCR

Primers and probes used in ddPCR assays were manually designed and synthetized by Integrated DNA Technologies, Inc. (IDT). Sequences of primers and probes are listed in Tables S5 and S6. All reactions were prepared using BioRad reagents and assays performed with BioRad equipment. After reverse transcription, ddPCR reaction solution was prepared to a final volume of 25 µl

containing 1x ddPCR supermix for probes, 250 nM gene specific primers, 125 nM probes (for ex-ON and ex-OFF), and cDNA (diluted from 20x to 40x). No template control and no reverse transcriptase control (RT-) were included in each ddPCR run to detect possible contaminations. The ddPCR reactions were loaded to a DG8 cartridge along with 70 µl of droplet generation oil to form droplets in a QX100 droplet generator. 40 µl of partitioned emulsion containing droplets was then slowly transferred to 96-Well twin Semi-Skirted PCR Plate (Eppendorf). After heat-sealing with foil, the plate containing the droplets was PCR cycled to the final point under conditions at 95°C, 10 min, 95°C 30 s and 60°C for 60 s for 40 cycles, 98°C for 10 min, then held at 4°C (for details about annealing temperature for each gene, please see Table S6). Following PCR, samples were read on a droplet reader which automatically reads the droplets from each well of the plate. Finally, data were analyzed using QuantaSoft software to determine the number of positive droplets. A manual selection of "+/-," "-/+," "+/+" and "-/-" counts was done using the Lasso function in the 2-D plots. The counts were then used by the software to calculate the copy numbers of FAM-positive droplets, HEX-positive, FAM- and HEX-double positive and negative droplets in the four quadrants. For each ddPCR assay serial dilutions of cDNA were used to obtain the lowest number of double-positive droplets; annealing temperature gradients were used to optimize PCR conditions and to determine the best separation between negative and positive reactions..

Assay for Repeat Expansion Transcripts

Reverse transcription was performed using 1 µg total RNA from compound-treated and untreated cells. PCR was carried out using 1/20 of the synthesized cDNA with primers N11, 5'-CACTGTCGGACATTCGGGAAGGTGC and 133, 5'GCTTGCACGTGTGGCTCAAGCAGCTG. For Genescan analysis primer N11 was labelled

with FAM. Amplification was performed with a Tm of 58^0C. The PCR product was subsequently heated to 95^0C for 2 minutes followed by cooling to 4^0C. For *Bpm*I restriction digestion analysis of *DMPK* PCR products, 8 μl of PCR mixture was digested overnight with restriction enzyme *Bpm*I (NEB) in a total reaction volume of 20 μl at 37^0C. The final products were analyzed by electrophoresis at 90V with 3% agarose gels and the density of bands quantified using ImageJ software or by fragment analysis on an ABI377 sequencer followed by Genescan quantification.

Western Blots and detection

Western blotting was performed using a commercial NuPage system (Invitrogen) according to the manufacturer's instructions. The primary antibodies used in this study were human CDK12 (Abcam, 1:400 dilution) and human α-tubulin (obtained from Santa Cruz and used at a dilution of 1:500). Anti-mouse IgG-horseradish peroxidise (HRP) was used as the secondary antibody. ImageJ software was used for the quantification of bands on western blots**.**

Immunohistochemistry studies

Cells were grown on coverslips for 24 hours before being fixed and permeabilized with 50:50 ice cold acetone:methanol. Cells were blocked in 5% BSA with 5% sheep serum. Anti-CDK12 antibody (Abcam) was used at 1:1000 dilution at 4ºC overnight followed by staining with Alexafluor-488 anti-mouse secondary antibody (1:500). Coverslips were mounted on slides using Vectorshield Mounting Media with DAPI. Images were acquired using a Zeiss 710 confocal microscope and analyzed using LSM image browser.

CDK12 shRNA knockdown and overexpression

Cells were plated at 40% confluency the day before infection in 96 well format. Lentiviral titre (SantaCruz sc-44343-V) was added at a multiplicity of infection (MOI) of 10 in 5μg/ml polybrene diluted in DMEM media. Cells were spin inoculated by centrifugation at 2500rpm for 30 minutes. Following 24 hours incubation the virus was removed and replaced with fresh DMEM media. The infection was repeated on day 4 and cells were collected on day 7 for immunohistochemistry and in situ hybridization analysis. For overexpression analysis cells were electroporated on day 1 with CDK12 full length open reading frame clone; BC150265 (GeneCopeoeia) and in situ hybridization conducted 48 hours later.

Transgenic mice

Homozygous human skeletal actin long repeat (*HSA*^{LR}) transgenic mice were previously described (*30*). Mice are routinely genotyped to confirm the presence of the CTG repeat expansion. *HSA*^{LR} mice, aged 8-12 weeks, housed in standard conditions, in groups of 4 in individual ventilated cages with standard laboratory food were used for EMG assessments (n = 12 males per group). They were randomly assigned to receive dinaciclib or vehicle alone (200 mg/ml 2-hydroxypropyl-beta-cyclodextrin, Sigma-Aldrich) by intraperitoneal injection at a 20mg/kg dose. Mice were dosed every other day for 4 injections and EMG was performed as previously described (*54*) by blinded examiner. Two mice were excluded from the treatment group due to adverse effects and 3 EMG data sets were excluded due to electrical interference. 1 day after the final injection mice were euthanized, muscle tissue was snap frozen and used for analysis of HSA transgene amounts and alternative splicing (8 samples were chosen at random from each group).

In situ hybridization of HSA^{LR} mouse muscle samples

8 female HSA^{LR}(12-17 weeks of age) were dosed 3 times with 20mg/kg of dinaciclib or vehicle alone (200 mg/ml 2-hydroxypropyl-beta-cyclodextrin, Sigma-Aldrich) by intraperitoneal injection over 24hrs. Mice were sacrificed 2 hrs after the final injection to allow assessment of dinaciclib on foci dissipation, in snap frozen gastrocnemius muscles samples. 12μm cryostat sections were thawed onto a Superfrost+ slide. Slides were fixed in 2% paraformaldehyde (PFA) in PBS for 30 minutes at 4°C. After 2 brief washes in PBS at room temperature slides were permeabilized in 2% acetone in PBS for 5 minutes at 4°C, followed by 2 brief washes in PBS. Prehybridization (2xSSC/30% formamide) was conducted at room temperature before hybridization at 42°C (2xSSC, 30% formamide, BSA, vanadate, 1mg/ml yeast tRNA, 500ng/ml Cy3-labelled $(CAG)_{10}$ probe) for 2 hours. Post-hybridization washes were in 2xSSC/30% formamide at 45°C for 30 minutes followed by 2xSSC at room temperatures for 5x5 minutes. Slides were incubated in PBS with 5mM $MgCl_2$ for 15 minutes at room temperature. After 2 brief washes in PBS/5mM $MgCl_2$ the stained sections were embedded in Vectashield and stored at 4°C.

Image Analysis

Microscopy was performed on a Zeiss 200M widefield fluorescence microscope using the DAPI filter for Hoechst stained nuclei and the TRITC filters for the CUG repeats detected with the Cy3 probe. Images were captured from 8 evenly spread locations with 20x objective as 16-bit Z stacks with 0.7μm step size over the full thickness of the sections for both the DAPI (nuclei) and the TRITC (CUG repeats) channel. Maximal (MAX) projection images were generated for both channels and nuclei selected using an IJ-Isodata threshold. Individual nuclei were segmented using rolling circle background subtraction and generated a binary mask to define the DAPI files. Background signal on the TRITC channel were subtracted from the signal generated using the

Triangle method. The two channels were merged to allow quantification of the relative amount of CAG probe signal per nuclei.

Assay to quantify transcription rates

Mouse P19 cells were treated with THZ531 at 300nM concentration for 24 hours prior to transfection (THZ531 was a gift from Nathanael Gray). Treated and untreated cells were transfected with pBItetDT960GFP (1.5μg) and pTet-One inducer plasmid (1μg) using Polyfect transfection reagent and transcription was induced with the addition of doxycycline to the media at 1μg/ml (pBItetDT960GFP was a gift from Thomas Cooper (Addgene plasmid # 80419)). 24 hours after induction cells were harvested and total RNA extracted. cDNA was synthesized using SuperScript III and processed by RT-PCR and ddPCR.

Nuclear Run-on Assay

Nuclear Run-on analysis was conducted following the protocol described in Gardini (2017) (*55*). KB Telo MyoD (DM1 fibroblasts) were used and transcript analysis was carried out using ddPCR, as described above.

Statistical Analysis

All raw data presented in this manuscript was assessed for normality using Shapiro-Wilk tests (or residuals in the case of analysis of variance (ANOVA) tests). Normally distributed data was tested for significance using two-tailed t tests, one or 2-way ANOVAs followed by Sidak's, Dunnet's or Tukey multiple comparison tests. Non-normal data was tested using a Mann Whitney test or Chi

squared analysis. P values were assumed to be significant if less than 0.05. Bonferroni correction was applied to the data in Figure 3D due to multiple testing which reduced the significant p value threshold to <0.005 for this dataset. Statistical tests were carried out using Graphpad Prism version 8.

Supplementary Materials

Supplementary Methods

Table S4: pIC50 values generated by affinity capturing with the SNS-032 affinity matrix in K562 cell extract for the different CDK inhibitors added to the cell extracts

Table S5: Dual-labeled probes used in ddPCR assays

Table S6: Primers used in ddPCR assays

Supplementary Dataset S1 (Excel document): Proteomic Raw Data

Supplementary Dataset S2 (Excel document): Whole Proteome and CZC188 beads DM vs non DM fibroblasts

Supplementary Dataset S3 (Excel document): Raw data and statistical details, Figures 1-5

References and Notes:

1. P. S. Harper, Myotonic Dystrophy. *Saunders, London, Philadelphia*, (2001).
2. J. D. Brook, M. E. Mccurrach, H. G. Harley, A. J. Buckler, D. Church, H. Aburatani, K. Hunter, V. P. Stanton, J. P. Thirion, T. Hudson, R. Sohn, B. Zemelman, R. G. Snell, S. A. Rundle, S. Crow, J. Davies, P. Shelbourne, J. Buxton, C. Jones, V. Juvonen, K. Johnson, P. S. Harper, D. J. Shaw, D. E. Housman, Molecular-Basis of Myotonic-Dystrophy - Expansion of a Trinucleotide (Ctg) Repeat at the 3' End of a Transcript Encoding a Protein-Kinase Family Member. *Cell* **68**, 799-808 (1992); published online EpubFeb 21 (
3. M. Mahadevan, C. Tsilfidis, L. Sabourin, G. Shutler, C. Amemiya, G. Jansen, C. Neville, M. Narang, J. Barcelo, K. Ohoy, S. Leblond, J. Earlemacdonald, P. J. Dejong, B. Wieringa, R. G. Korneluk, Myotonic-Dystrophy Mutation - an Unstable Ctg Repeat in the 3' Untranslated Region of the Gene. *Science* **255**, 1253-1255 (1992); published online EpubMar 6 (
4. Y. H. Fu, A. Pizzuti, R. G. Fenwick, J. King, S. Rajnarayan, P. W. Dunne, J. Dubel, G. A. Nasser, T. Ashizawa, P. Dejong, B. Wieringa, R. Korneluk, M. B. Perryman, H. F. Epstein, C. T. Caskey, An Unstable Triplet Repeat in a Gene Related to Myotonic Muscular-Dystrophy. *Science* **255**, 1256-1258 (1992); published online EpubMar 6 (
5. B. M. Davis, M. E. McCurrach, K. L. Taneja, R. H. Singer, D. E. Housman, Expansion of a CUG trinucleotide repeat in the 3' untranslated region of myotonic dystrophy protein kinase transcripts results in nuclear retention of transcripts. *Proceedings of the National Academy of Sciences of the United States of America* **94**, 7388-7393 (1997); published online EpubJul 8 (
6. K. L. Taneja, M. Mccurrach, M. Schalling, D. Housman, R. H. Singer, Foci of Trinucleotide Repeat Transcripts in Nuclei of Myotonic-Dystrophy Cells and Tissues. *J Cell Biol* **128**, 995-1002 (1995); published online EpubMar (DOI 10.1083/jcb.128.6.995).
7. M. G. Hamshere, E. E. Newman, M. Alwazzan, B. S. Athwal, J. D. Brook, Transcriptional abnormality in myotonic dystrophy affects DMPK but not neighboring genes. *Proceedings of the National Academy of Sciences of the United States of America* **94**, 7394-7399 (1997); published online EpubJul 8 (
8. A. Mankodi, C. R. Urbinati, Q. P. Yuan, R. T. Moxley, V. Sansone, M. Krym, D. Henderson, M. Schalling, M. S. Swanson, C. A. Thornton, Muscleblind localizes to nuclear foci of aberrant RNA in myotonic dystrophy types 1 and 2. *Human molecular genetics* **10**, 2165-2170 (2001); published online EpubSep 15 (
9. M. Fardaei, K. Larkin, J. D. Brook, M. G. Hamshere, In vivo co-localisation of MBNL protein with DMPK expanded-repeat transcripts. *Nucleic Acids Res* **29**, 2766-2771 (2001); published online EpubJul 1 (

10. N. M. Kuyumcu-Martinez, G. S. Wang, T. A. Cooper, Increased steady-state levels of CUGBP1 in myotonic dystrophy 1 are due to PKC-mediated hyperphosphorylation. *Mol Cell* **28**, 68-78 (2007); published online EpubOct 12 (S1097-2765(07)00544-8 [pii]
10.1016/j.molcel.2007.07.027).
11. C. Huichalaf, B. Schoser, C. Schneider-Gold, B. Jin, P. Sarkar, L. Timchenko, Reduction of the rate of protein translation in patients with myotonic dystrophy 2. *The Journal of neuroscience : the official journal of the Society for Neuroscience* **29**, 9042-9049 (2009); published online EpubJul 15 (10.1523/JNEUROSCI.1983-09.2009).
12. T. Zu, B. Gibbens, N. S. Doty, M. Gomes-Pereira, A. Huguet, M. D. Stone, J. Margolis, M. Peterson, T. W. Markowski, M. A. Ingram, Z. Nan, C. Forster, W. C. Low, B. Schoser, N. V. Somia, H. B. Clark, S. Schmechel, P. B. Bitterman, G. Gourdon, M. S. Swanson, M. Moseley, L. P. Ranum, Non-ATG-initiated translation directed by microsatellite expansions. *Proceedings of the National Academy of Sciences of the United States of America* **108**, 260-265 (2011); published online EpubJan 4 (10.1073/pnas.1013343108).
13. E. L. Logigian, W. B. Martens, R. T. t. Moxley, M. P. McDermott, N. Dilek, A. W. Wiegner, A. T. Pearson, C. A. Barbieri, C. L. Annis, C. A. Thornton, R. T. Moxley, 3rd, Mexiletine is an effective antimyotonia treatment in myotonic dystrophy type 1. *Neurology* **74**, 1441-1448 (2010); published online EpubMay 4 (10.1212/WNL.0b013e3181dc1a3a).
14. D. Hilton-Jones, M. Bowler, H. Lochmueller, C. Longman, R. Petty, M. Roberts, M. Rogers, C. Turner, D. Wilcox, Modafinil for excessive daytime sleepiness in myotonic dystrophy type 1--the patients' perspective. *Neuromuscular disorders : NMD* **22**, 597-603 (2012); published online EpubJul (10.1016/j.nmd.2012.02.005).
15. M. A. Langlois, N. S. Lee, J. J. Rossi, J. Puymirat, Hammerhead ribozyme-mediated destruction of nuclear foci in myotonic dystrophy myoblasts. *Molecular therapy : the journal of the American Society of Gene Therapy* **7**, 670-680 (2003); published online EpubMay (
16. S. A. Mulders, W. J. van den Broek, T. M. Wheeler, H. J. Croes, P. van Kuik-Romeijn, S. J. de Kimpe, D. Furling, G. J. Platenburg, G. Gourdon, C. A. Thornton, B. Wieringa, D. G. Wansink, Triplet-repeat oligonucleotide-mediated reversal of RNA toxicity in myotonic dystrophy. *Proceedings of the National Academy of Sciences of the United States of America* **106**, 13915-13920 (2009); published online EpubAug 18 (0905780106 [pii]
10.1073/pnas.0905780106).
17. T. M. Wheeler, A. J. Leger, S. K. Pandey, A. R. MacLeod, M. Nakamori, S. H. Cheng, B. M. Wentworth, C. F. Bennett, C. A. Thornton, Targeting nuclear RNA for in vivo correction of myotonic dystrophy. *Nature* **488**, 111-115; published online EpubAug 2 (nature11362 [pii]
10.1038/nature11362).
18. M. B. Warf, M. Nakamori, C. M. Matthys, C. A. Thornton, J. A. Berglund, Pentamidine reverses the splicing defects associated with myotonic dystrophy. *Proceedings of the National Academy of Sciences of the United States of America* **106**, 18551-18556 (2009); published online EpubNov 3 (10.1073/pnas.0903234106).
19. C. H. Wong, L. Nguyen, J. Peh, L. M. Luu, J. S. Sanchez, S. L. Richardson, T. Tuccinardi, H. Tsoi, W. Y. Chan, H. Y. Chan, A. M. Baranger, P. J. Hergenrother, S. C. Zimmerman, Targeting Toxic RNAs that Cause Myotonic Dystrophy Type 1 (DM1) with a Bisamidinium Inhibitor. *Journal of the American Chemical Society*, (2014); published online EpubApr 4 (10.1021/ja5012146).
20. J. L. Childs-Disney, R. Parkesh, M. Nakamori, C. A. Thornton, M. D. Disney, Rational design of bioactive, modularly assembled aminoglycosides targeting the RNA that causes myotonic dystrophy type 1. *ACS chemical biology* **7**, 1984-1993 (2012); published online EpubDec 21 (10.1021/cb3001606).
21. J. W. Hoskins, L. O. Ofori, C. Z. Chen, A. Kumar, K. Sobczak, M. Nakamori, N. Southall, S. Patnaik, J. J. Marugan, W. Zheng, C. P. Austin, M. D. Disney, B. L. Miller, C. A. Thornton, Lomofungin and dilomofungin: inhibitors of MBNL1-CUG RNA binding with distinct cellular effects. *Nucleic Acids Res* **42**, 6591-6602 (2014)10.1093/nar/gku275).
22. A. Ketley, C. Z. Chen, X. Li, S. Arya, T. E. Robinson, J. Granados-Riveron, I. Udosen, G. E. Morris, I. Holt, D. Furling, S. Chaouch, B. Haworth, N. Southall, P. Shinn, W. Zheng, C. P. Austin, C. J. Hayes, J. D. Brook, High-content screening identifies small molecules that remove nuclear foci, affect MBNL distribution and CELF1 protein levels via a PKC-independent pathway in myotonic dystrophy cell lines. *Human molecular genetics* **23**, 1551-1562 (2014); published online EpubMar 15 (10.1093/hmg/ddt542).
23. D. H. Drewry, T. M. Willson, W. J. Zuercher, Seeding collaborations to advance kinase science with the GSK Published Kinase Inhibitor Set (PKIS). *Current topics in medicinal chemistry* **14**, 340-342 (2014).

24. P. Ghia, L. Scarfo, S. Perez, K. Pathiraja, M. Derosier, K. Small, C. McCrary Sisk, N. Patton, Efficacy and safety of dinaciclib vs ofatumumab in patients with relapsed/refractory chronic lymphocytic leukemia. *Blood* **129**, 1876-1878 (2017); published online EpubMar 30 (10.1182/blood-2016-10-748210).
25. S. K. Kumar, B. LaPlant, W. J. Chng, J. Zonder, N. Callander, R. Fonseca, B. Fruth, V. Roy, C. Erlichman, A. K. Stewart, C. Mayo Phase, Dinaciclib, a novel CDK inhibitor, demonstrates encouraging single-agent activity in patients with relapsed multiple myeloma. *Blood* **125**, 443-448 (2015); published online EpubJan 15 (10.1182/blood-2014-05-573741).
26. J. Flynn, J. Jones, A. J. Johnson, L. Andritsos, K. Maddocks, S. Jaglowski, J. Hessler, M. R. Grever, E. Im, H. Zhou, Y. Zhu, D. Zhang, K. Small, R. Bannerji, J. C. Byrd, Dinaciclib is a novel cyclin-dependent kinase inhibitor with significant clinical activity in relapsed and refractory chronic lymphocytic leukemia. *Leukemia* **29**, 1524-1529 (2015); published online EpubJul (10.1038/leu.2015.31).
27. W. G. Tong, R. Chen, W. Plunkett, D. Siegel, R. Sinha, R. D. Harvey, A. Z. Badros, L. Popplewell, S. Coutre, J. A. Fox, K. Mahadocon, T. Chen, P. Kegley, U. Hoch, W. G. Wierda, Phase I and pharmacologic study of SNS-032, a potent and selective Cdk2, 7, and 9 inhibitor, in patients with advanced chronic lymphocytic leukemia and multiple myeloma. *Journal of clinical oncology : official journal of the American Society of Clinical Oncology* **28**, 3015-3022 (2010); published online EpubJun 20 (10.1200/JCO.2009.26.1347).
28. E. I. Heath, K. Bible, R. E. Martell, D. C. Adelman, P. M. Lorusso, A phase 1 study of SNS-032 (formerly BMS-387032), a potent inhibitor of cyclin-dependent kinases 2, 7 and 9 administered as a single oral dose and weekly infusion in patients with metastatic refractory solid tumors. *Investigational new drugs* **26**, 59-65 (2008); published online EpubFeb (10.1007/s10637-007-9090-3).
29. D. Parry, T. Guzi, F. Shanahan, N. Davis, D. Prabhavalkar, D. Wiswell, W. Seghezzi, K. Paruch, M. P. Dwyer, R. Doll, A. Nomeir, W. Windsor, T. Fischmann, Y. Wang, M. Oft, T. Chen, P. Kirschmeier, E. M. Lees, Dinaciclib (SCH 727965), a novel and potent cyclin-dependent kinase inhibitor. *Molecular cancer therapeutics* **9**, 2344-2353 (2010); published online EpubAug (10.1158/1535-7163.MCT-10-0324).
30. A. Mankodi, E. Logigian, L. Callahan, C. McClain, R. White, D. Henderson, M. Krym, C. A. Thornton, Myotonic dystrophy in transgenic mice expressing an expanded CUG repeat. *Science* **289**, 1769-1773 (2000); published online EpubSep 08 (
31. T. M. Wheeler, J. D. Lueck, M. S. Swanson, R. T. Dirksen, C. A. Thornton, Correction of ClC-1 splicing eliminates chloride channelopathy and myotonia in mouse models of myotonic dystrophy. *J Clin Invest* **117**, 3952-3957 (2007); published online EpubDec (10.1172/JCI33355).
32. X. Lin, J. W. Miller, A. Mankodi, R. N. Kanadia, Y. Yuan, R. T. Moxley, M. S. Swanson, C. A. Thornton, Failure of MBNL1-dependent post-natal splicing transitions in myotonic dystrophy. *Human molecular genetics* **15**, 2087-2097 (2006); published online EpubJul 1 (10.1093/hmg/ddl132).
33. M. Wojciechowska, K. Sobczak, P. Kozlowski, S. Sedehizadeh, A. Wojtkowiak-Szlachcic, K. Czubak, R. Markus, A. Lusakowska, A. Kaminska, J. D. Brook, Quantitative Methods to Monitor RNA Biomarkers in Myotonic Dystrophy. *Sci Rep* **8**, 5885 (2018); published online EpubApr 12 (10.1038/s41598-018-24156-x).
34. D. M. Dixon, J. Choi, A. El-Ghazali, S. Y. Park, K. P. Roos, M. C. Jordan, M. C. Fishbein, L. Comai, S. Reddy, Loss of muscleblind-like 1 results in cardiac pathology and persistence of embryonic splice isoforms. *Sci Rep* **5**, 9042 (2015); published online EpubMar 12 (10.1038/srep09042).
35. Y. Yamashita, T. Matsuura, T. Kurosaki, Y. Amakusa, M. Kinoshita, T. Ibi, K. Sahashi, K. Ohno, LDB3 splicing abnormalities are specific to skeletal muscles of patients with myotonic dystrophy type 1 and alter its PKC binding affinity. *Neurobiol Dis* **69**, 200-205 (2014); published online EpubSep (10.1016/j.nbd.2014.05.026).
36. K. Charizanis, K. Y. Lee, R. Batra, M. Goodwin, C. Zhang, Y. Yuan, L. Shiue, M. Cline, M. M. Scotti, G. Xia, A. Kumar, T. Ashizawa, H. B. Clark, T. Kimura, M. P. Takahashi, H. Fujimura, K. Jinnai, H. Yoshikawa, M. Gomes-Pereira, G. Gourdon, N. Sakai, S. Nishino, T. C. Foster, M. Ares, Jr., R. B. Darnell, M. S. Swanson, Muscleblind-like 2-mediated alternative splicing in the developing brain and dysregulation in myotonic dystrophy. *Neuron* **75**, 437-450 (2012); published online EpubAug 9 (10.1016/j.neuron.2012.05.029).
37. S. D. Wagner, A. J. Struck, R. Gupta, D. R. Farnsworth, A. E. Mahady, K. Eichinger, C. A. Thornton, E. T. Wang, J. A. Berglund, Dose-Dependent Regulation of Alternative Splicing by MBNL Proteins Reveals Biomarkers for Myotonic Dystrophy. *PLoS Genet* **12**, e1006316 (2016); published online EpubSep (10.1371/journal.pgen.1006316).
38. M. Bantscheff, D. Eberhard, Y. Abraham, S. Bastuck, M. Boesche, S. Hobson, T. Mathieson, J. Perrin, M. Raida, C. Rau, V. Reader, G. Sweetman, A. Bauer, T. Bouwmeester, C. Hopf, U. Kruse, G. Neubauer, N. Ramsden, J. Rick, B. Kuster, G. Drewes, Quantitative chemical proteomics reveals mechanisms of action of

clinical ABL kinase inhibitors. *Nature biotechnology* **25**, 1035-1044 (2007); published online EpubSep (10.1038/nbt1328).
39. T. Werner, I. Becher, G. Sweetman, C. Doce, M. M. Savitski, M. Bantscheff, High-resolution enabled TMT 8-plexing. *Analytical chemistry* **84**, 7188-7194 (2012); published online EpubAug 21 (10.1021/ac301553x).
40. U. Kruse, C. P. Pallasch, M. Bantscheff, D. Eberhard, L. Frenzel, S. Ghidelli, S. K. Maier, T. Werner, C. M. Wendtner, G. Drewes, Chemoproteomics-based kinome profiling and target deconvolution of clinical multi-kinase inhibitors in primary chronic lymphocytic leukemia cells. *Leukemia* **25**, 89-100 (2011); published online EpubJan (Doi 10.1038/Leu.2010.233).
41. G. Bergamini, K. Bell, S. Shimamura, T. Werner, A. Cansfield, K. Muller, J. Perrin, C. Rau, K. Ellard, C. Hopf, C. Doce, D. Leggate, R. Mangano, T. Mathieson, A. O'Mahony, I. Plavec, F. Rharbaoui, F. Reinhard, M. M. Savitski, N. Ramsden, E. Hirsch, G. Drewes, O. Rausch, M. Bantscheff, G. Neubauer, A selective inhibitor reveals PI3Kgamma dependence of T(H)17 cell differentiation. *Nature chemical biology* **8**, 576-582 (2012); published online EpubJun (10.1038/nchembio.957).
42. T. K. Ko, E. Kelly, J. Pines, CrkRS: a novel conserved Cdc2-related protein kinase that colocalises with SC35 speckles. *Journal of cell science* **114**, 2591-2603 (2001); published online EpubJul (
43. I. Holt, S. Mittal, D. Furling, G. S. Butler-Browne, J. D. Brook, G. E. Morris, Defective mRNA in myotonic dystrophy accumulates at the periphery of nuclear splicing speckles. *Neuromuscular Disord* **18**, 798-799 (2008); published online EpubOct (10.1016/j.nmd.2008.06.257).
44. B. Bartkowiak, P. Liu, H. P. Phatnani, N. J. Fuda, J. J. Cooper, D. H. Price, K. Adelman, J. T. Lis, A. L. Greenleaf, CDK12 is a transcription elongation-associated CTD kinase, the metazoan ortholog of yeast Ctk1. *Genes & development* **24**, 2303-2316 (2010); published online EpubOct 15 (10.1101/gad.1968210).
45. J. E. Lee, C. F. Bennett, T. A. Cooper, RNase H-mediated degradation of toxic RNA in myotonic dystrophy type 1. *Proceedings of the National Academy of Sciences of the United States of America* **109**, 4221-4226 (2012); published online EpubMar 13 (10.1073/pnas.1117019109).
46. T. Zhang, N. Kwiatkowski, C. M. Olson, S. E. Dixon-Clarke, B. J. Abraham, A. K. Greifenberg, S. B. Ficarro, J. M. Elkins, Y. Liang, N. M. Hannett, T. Manz, M. Hao, B. Bartkowiak, A. L. Greenleaf, J. A. Marto, M. Geyer, A. N. Bullock, R. A. Young, N. S. Gray, Covalent targeting of remote cysteine residues to develop CDK12 and CDK13 inhibitors. *Nature chemical biology* **12**, 876-884 (2016); published online EpubOct (10.1038/nchembio.2166).
47. C. A. Bosken, L. Farnung, C. Hintermair, M. Merzel Schachter, K. Vogel-Bachmayr, D. Blazek, K. Anand, R. P. Fisher, D. Eick, M. Geyer, The structure and substrate specificity of human Cdk12/Cyclin K. *Nature communications* **5**, 3505 (2014)10.1038/ncomms4505).
48. D. Ostapenko, M. J. Solomon, Phosphorylation by Cak1 regulates the C-terminal domain kinase Ctk1 in Saccharomyces cerevisiae. *Molecular and cellular biology* **25**, 3906-3913 (2005); published online EpubMay (10.1128/MCB.25.10.3906-3913.2005).
49. T. Wang, K. Birsoy, N. W. Hughes, K. M. Krupczak, Y. Post, J. J. Wei, E. S. Lander, D. M. Sabatini, Identification and characterization of essential genes in the human genome. *Science* **350**, 1096-1101 (2015); published online EpubNov 27 (10.1126/science.aac7041).
50. D. Blazek, J. Kohoutek, K. Bartholomeeusen, E. Johansen, P. Hulinkova, Z. Luo, P. Cimermancic, J. Ule, B. M. Peterlin, The Cyclin K/Cdk12 complex maintains genomic stability via regulation of expression of DNA damage response genes. *Genes & development* **25**, 2158-2172 (2011); published online EpubOct 15 (10.1101/gad.16962311).
51. X. Li, N. Chatterjee, K. Spirohn, M. Boutros, D. Bohmann, Cdk12 Is A Gene-Selective RNA Polymerase II Kinase That Regulates a Subset of the Transcriptome, Including Nrf2 Target Genes. *Sci Rep* **6**, 21455 (2016); published online EpubFeb 25 (10.1038/srep21455).
52. R. N. Kanadia, J. Shin, Y. Yuan, S. G. Beattie, T. M. Wheeler, C. A. Thornton, M. S. Swanson, Reversal of RNA missplicing and myotonia after muscleblind overexpression in a mouse poly(CUG) model for myotonic dystrophy. *Proceedings of the National Academy of Sciences of the United States of America* **103**, 11748-11753 (2006); published online EpubAug 1 (10.1073/pnas.0604970103).
53. M. Bantscheff, C. Hopf, M. M. Savitski, A. Dittmann, P. Grandi, A. M. Michon, J. Schlegl, Y. Abraham, I. Becher, G. Bergamini, M. Boesche, M. Delling, B. Dumpelfeld, D. Eberhard, C. Huthmacher, T. Mathieson, D. Poeckel, V. Reader, K. Strunk, G. Sweetman, U. Kruse, G. Neubauer, N. G. Ramsden, G. Drewes, Chemoproteomics profiling of HDAC inhibitors reveals selective targeting of HDAC complexes. *Nature biotechnology* **29**, 255-265 (2011); published online EpubMar (10.1038/nbt.1759).

54. T. M. Wheeler, A. J. Leger, S. K. Pandey, A. R. MacLeod, M. Nakamori, S. H. Cheng, B. M. Wentworth, C. F. Bennett, C. A. Thornton, Targeting nuclear RNA for in vivo correction of myotonic dystrophy. *Nature* **488**, 111-115 (2012); published online EpubAug 02 (10.1038/nature11362).
55. A. Gardini, Global Run-On Sequencing (GRO-Seq). *Methods in molecular biology* **1468**, 111-120 (2017)10.1007/978-1-4939-4035-6_9).
56. M. M. Savitski, F. Fischer, T. Mathieson, G. Sweetman, M. Lang, M. Bantscheff, Targeted data acquisition for improved reproducibility and robustness of proteomic mass spectrometry assays. *Journal of the American Society for Mass Spectrometry* **21**, 1668-1679 (2010); published online EpubOct (10.1016/j.jasms.2010.01.012).
57. M. M. Savitski, T. Mathieson, N. Zinn, G. Sweetman, C. Doce, I. Becher, F. Pachl, B. Kuster, M. Bantscheff, Measuring and managing ratio compression for accurate iTRAQ/TMT quantification. *Journal of proteome research* **12**, 3586-3598 (2013); published online EpubAug 2 (10.1021/pr400098r).
58. W. K.M. Chong, S.S. Chu, R.K. Duvadie, L. Li, W. Xiao, Y. Yang. WO 9921845 [Patent] 4-aminothiazole derivatives, their preparation and their use as inhibitors of cyclin-dependent kinases.
59. P. G. Wyatt, A. J. Woodhead, V. Berdini, J. A. Boulstridge, M. G. Carr, D. M. Cross, D. J. Davis, L. A. Devine, T. R. Early, R. E. Feltell, E. J. Lewis, R. L. McMenamin, E. F. Navarro, M. A. O'Brien, M. O'Reilly, M. Reule, G. Saxty, L. C. Seavers, D. M. Smith, M. S. Squires, G. Trewartha, M. T. Walker, A. J. Woolford, Identification of N-(4-piperidinyl)-4-(2,6-dichlorobenzoylamino)-1H-pyrazole-3-carboxamide (AT7519), a novel cyclin dependent kinase inhibitor using fragment-based X-ray crystallography and structure based drug design. Journal of medicinal chemistry 51, 4986-4999 (2008)
60. K. Paruch, M. P. Dwyer, C. Alvarez, C. Brown, T. Y. Chan, R. J. Doll, K. Keertikar, C. Knutson, B. McKittrick, J. Rivera, R. Rossman, G. Tucker, T. Fischmann, A. Hruza, V. Madison, A. A. Nomeir, Y. Wang, P. Kirschmeier, E. Lees, D. Parry, N. Sgambellone, W. Seghezzi, L. Schultz, F. Shanahan, D. Wiswell, X. Xu, Q. Zhou, R. A. James, V. M. Paradkar, H. Park, L. R. Rokosz, T. M. Stauffer, T. J. Guzi, Discovery of Dinaciclib (SCH 727965): A Potent and Selective Inhibitor of Cyclin-Dependent Kinases. ACS medicinal chemistry letters 1, 204-208 (2010)
61. J. M. Elkins, V. Fedele, M. Szklarz, K. R. Abdul Azeez, E. Salah, J. Mikolajczyk, S. Romanov, N. Sepetov, X. P. Huang, B. L. Roth, A. Al Haj Zen, D. Fourches, E. Muratov, A. Tropsha, J. Morris, B. A. Teicher, M. Kunkel, E. Polley, K. E. Lackey, F. L. Atkinson, J. P. Overington, P. Bamborough, S. Muller, D. J. Price, T. M. Willson, D. H. Drewry, S. Knapp, W. J. Zuercher, Comprehensive characterization of the Published Kinase Inhibitor Set. Nature biotechnology 34, 95-103 (2016)
62. K. L. Stevens, M. J. Reno, J. B. Alberti, D. J. Price, L. S. Kane-Carson, V. B. Knick, L. M. Shewchuk, A. M. Hassell, J. M. Veal, S. T. Davis, R. J. Griffin, M. R. Peel, Synthesis and evaluation of pyrazolo[1,5-b]pyridazines as selective cyclin dependent kinase inhibitors. Bioorganic & medicinal chemistry letters 18, 5758-5762 (2008)
63. P. L. Toogood, P. J. Harvey, J. T. Repine, D. J. Sheehan, S. N. VanderWel, H. Zhou, P. R. Keller, D. J. McNamara, D. Sherry, T. Zhu, J. Brodfuehrer, C. Choi, M. R. Barvian, D. W. Fry, Discovery of a potent and selective inhibitor of cyclin-dependent kinase 4/6. Journal of medicinal chemistry 48, 2388-2406 (2005)
64. R. N. Misra, H. Y. Xiao, K. S. Kim, S. Lu, W. C. Han, S. A. Barbosa, J. T. Hunt, D. B. Rawlins, W. Shan, S. Z. Ahmed, L. Qian, B. C. Chen, R. Zhao, M. S. Bednarz, K. A. Kellar, J. G. Mulheron, R. Batorsky, U. Roongta, A. Kamath, P. Marathe, S. A. Ranadive, J. S. Sack, J. S. Tokarski, N. P. Pavletich, F. Y. Lee, K. R. Webster, S. D. Kimball, N-(cycloalkylamino)acyl-2-aminothiazole inhibitors of cyclin-dependent kinase 2. N-[5-[[[5-(1,1-dimethylethyl)-2-oxazolyl]methyl]thio]-2-thiazolyl]-4- piperidinecarboxamide (BMS-387032), a highly efficacious and selective antitumor agent. Journal of medicinal chemistry 47, 1719-1728 (2004)
65. C. B. Baltus, R. Jorda, C. Marot, K. Berka, V. Bazgier, V. Krystof, G. Prie, M. C. Viaud-Massuard, Synthesis, biological evaluation and molecular modeling of a novel series of 7-azaindole based tri-heterocyclic compounds as potent CDK2/Cyclin E inhibitors. European journal of medicinal chemistry 108, 701-719 (2016)
66. M. S. Squires, R. E. Feltell, N. G. Wallis, E. J. Lewis, D. M. Smith, D. M. Cross, J. F. Lyons, N. T. Thompson, Biological characterization of AT7519, a small-molecule inhibitor of cyclin-dependent kinases, in human tumor cell lines. Molecular cancer therapeutics 8, 324-332 (2009)
67. A. Conroy, D. E. Stockett, D. Walker, M. R. Arkin, U. Hoch, J. A. Fox, R. E. Hawtin, SNS-032 is a potent and selective CDK 2, 7 and 9 inhibitor that drives target modulation in patient samples. Cancer chemotherapy and pharmacology 64, 723-732 (2009)
68. P.W. 2002012250

69. D. W. Fry, P. J. Harvey, P. R. Keller, W. L. Elliott, M. Meade, E. Trachet, M. Albassam, X. Zheng, W. R. Leopold, N. K. Pryer, P. L. Toogood, Specific inhibition of cyclin-dependent kinase 4/6 by PD 0332991 and associated antitumor activity in human tumor xenografts. Molecular cancer therapeutics 3, 1427-1438 (2004)
70. J. T. Metz, E. F. Johnson, N. B. Soni, P. J. Merta, L. Kifle, P. J. Hajduk, Navigating the kinome. Nature chemical biology 7, 200-202 (2011)
71. L. Meijer, A. Borgne, O. Mulner, J. P. Chong, J. J. Blow, N. Inagaki, M. Inagaki, J. G. Delcros, J. P. Moulinoux, Biochemical and cellular effects of roscovitine, a potent and selective inhibitor of the cyclin-dependent kinases cdc2, cdk2 and cdk5. European journal of biochemistry 243, 527-536 (1997)
72. P. Rickert, J. L. Corden, E. Lees, Cyclin C/CDK8 and cyclin H/CDK7/p36 are biochemically distinct CTD kinases. Oncogene 18, 1093-1102 (1999)
73. S. J. McClue, D. Blake, R. Clarke, A. Cowan, L. Cummings, P. M. Fischer, M. MacKenzie, J. Melville, K. Stewart, S. Wang, N. Zhelev, D. Zheleva, D. P. Lane, In vitro and in vivo antitumor properties of the cyclin dependent kinase inhibitor CYC202 (R-roscovitine). International journal of cancer 102, 463-468 (2002)

Acknowledgments: We would like to thank T. Self, M. Jundt and K. Kammerer for expert technical assistance. We would like to thank N.Gray and T.Cooper for providing valuable reagents and the volunteers who gave muscle biopsies for analysis.

Funding: This work was supported by the University of Nottingham Hermes fellowship award (AK), Myotonic Dystrophy Support Group (JDB), Marigold Foundation (JDB), Muscular Dystrophy Campaign (JDB), The People Programme (Marie Curie Actions) of the European Union's Seventh Framework Programme (FP7/2007-2013) under REA grants agreement No PCOFUND-GA-2012-600181 (MW) and the Polish National Science Center (2014/13/B/NZ5/03214 to MW), NIH grant NS048843 (CAT), Wellcome Trust [grant number 107562/Z/15/Z; 2015] (JDB, CJH and RCT) and The British Heart Foundation [grant number RG/13/10/30376] (JDB). The SGC is a registered charity (number 1097737) that receives funds from AbbVie, Bayer Pharma AG, Boehringer Ingelheim, Canada Foundation for Innovation, Eshelman Institute for Innovation, Genome Canada, Innovative Medicines Initiative (EU/EFPIA), Janssen, Merck & Co., Novartis Pharma AG, Ontario Ministry of Economic Development and Innovation, Pfizer, São Paulo Research Foundation-FAPESP, Takeda, and Wellcome Trust.

Author contributions: Assay Development: AK, MW, MR, DD, WJZ, GD, IU, CJH, JDB. Performed experiments: Fig. 1: AK Fig. 2: AK, MW Fig. 3: MW, RBC, RCT, PCG, AA, OO Fig. 4: SGD, MB, Fig. 5: AK, MW, TKG, MLM, SS, NAM, JDB. Suppl. figs: AK, MW, SGD, ZT, PP, MT, MB, CAT. Data analysis and interpretation: AK, SGD, MW, PB, RBC, RCT, MB, MR, DEM, DHD, WJZ, GD, IU, CJH, JDB. Wrote the manuscript: AK, WJZ, GD, IU, CJH, JDB.

Competing interests: SGD, PB, MB, MB, MR, DEM, DHD, WJZ, GD, and IU are employees and/or shareholders of Cellzome GmbH and GlaxoSmithKline. The University of Nottingham has applied for a patent relating to this work (Inhibitors and their uses, WO 2017/163076 A1).

Data and materials availability

THZ531 is available from Dr Nathanael Gray under a material transfer agreement with the University of Nottingham. All the data used for this manuscript are in the main text or supplementary material.

Figure Legends

Fig. 1. Screening of the PKIS compound collection using the nuclear foci assay

(A-F) Graphs show percentage of nuclear foci relative to DMSO-treated cells across a dilution series. Average foci number in DMSO-treated cells=4.09; SD=0.78. All six compounds share a pyrazolo[1,5b]pyridazine core structure (**A**) GW778894X (**B**) GW779439X (**C**) GW780056X (**D**) GW810576X (**E**) GW806290X (**F**) GW801372X (**G**) Loading plot of 2-component partial least squares model. Kinase activities correlating with the nuclear foci assay are labelled, with cyclin-dependent kinases highlighted in red. (**H**) Nuclear foci quantification in DM1 fibroblast cells following dinaciclib treatment. (**I**) Nuclear foci quantification in DM1 fibroblast cells following SNS-032 treatment.

Fig. 2. Inhibitor treatment as a therapeutic for DM1

(**A-D**) Histograms show percentage of cells in the population with 0, <2, <5 and ≥5 foci per nucleus (**A)** Untreated DM1 cells. (**B)** DM1 cells treated with SNS-032 for 2 hours. (**C)** DM1 cells treated with SNS-032 for 2 hours with 48 hours recovery in growth media. (**D)** DM1 cells treated with SNS-032 for 2 hours with 72 hours recovery in growth media. (Chi squared test, $p<0.0001$) (**E**) Ethidium bromide stained gel showing RT-PCR products from nuclear (N) and cytoplasmic (C) RNA fractions following amplification and *Bpm*I digest of a fragment of *DMPK*. *GAPDH* is used as a loading control. (**F)** Histograms showing the relative proportions of nuclear mutant *DMPK* transcripts compared to wild type *DMPK* transcripts. The *Bpm*I polymorphism was used to distinguish copy number of mutant and wild type transcripts of *DMPK*. (2 way ANOVA, Sidak post-hoc: treatment vs control for wild type transcript: ns. treatment vs control for mutant transcript: p<00001, *N=3-4*) (**G-H)** ddPCR on total RNA from KB Telo MyoD (*N=4*-5) (**G**) KB

with dinaciclib (2 way ANOVA: Sidak post-hoc: Wildtype transcript; treatment vs DMSO: ns. Mutant transcript; treatment vs DMSO, p <0.0001.) (**H**) KB with SNS-032 (Sidak post-hoc: Wildtype transcript; treatment vs DMSO: ns. Mutant transcript; treatment vs DMSO, p = 0.043) and (**I-J**) HK Telo MyoD (*N*=5). (**I)** HK with dinaciclib (2 way ANOVA: Sidak post-hoc: Wildtype transcript; treatment vs DMSO: ns. Mutant transcript; treatment vs DMSO, p <0.0001.) (**J)** HK with SNS-032 (Sidak post-hoc: Wildtype transcript; treatment vs DMSO, p<0.0015. Mutant transcript; treatment vs DMSO, p <0.0001.) Cells were treated with 1μM dinaciclib and 0.15μM SNS-032 for 24 hours. Bars show mean ± SD. p values of <0.05 were considered to be statistically significant.

Fig. 3. Inhibitor treatment in a DM1 mouse model

(A) Example images showing sections of gastrocnemius muscle from vehicle treated and dinaciclib HSA^{LR} treated mice following in situ hybridization to detect nuclear foci. (**B**) Nuclear foci fluorescent signal intensity in vehicle and dinaciclib treated HSA^{LR} mice (Two tailed t-test p=0.0052, *N*=4 animals per treatment group) (**C**) HSA transgene amount was quantified by ddPCR following vehicle and dinaciclib treatments (Two-tailed t-test, p<0.0001, 8 animals per treatment group) **(D)** 9 key splice isoforms were analyzed in gastrocnemius muscle samples from vehicle and dinaciclib treated mice (two tailed student t test and Mann-Whitney testing for non-normal data; Bonferroni correction applied and p values of <0.005 were considered significant) **(E)** Myotonia grade scores in gastrocnemius muscle from HSA^{LR} mice following vehicle and dinaciclib compound treatment (n=9-10 per treatment group; Mann-Whitney; p=0.0443, p values of <0.05 were considered significant). Myotonia was performed by blinded examiner and graded as follows: 0 indicates no myotonia; 1, occasional myotonic discharge in less than 50% of electrode

insertions; 2, myotonic discharge in greater than 50% of insertions; 3, myotonic discharge with nearly every insertion. Wild-type mice of the same inbred strain background (FVB) do not show myotonia. Bars show mean ± SD.

Fig. 4. Chemoproteomics target deconvolution

IC_{50} values were generated by affinity capturing of kinases (**A**) CDK1 (**B**) CDK2 (**C**) CDK4 (**D**) CDK5 (**E**) CDK6 (**F**) CDK7 (**G**) CDK9 (**H**) CDK10 (**I**) CDK12 (**J**) CDK13 (**K**) PCTK1 (**L**) PCTK2 from K562 or A204 cell extract using beads derivatized with SNS-032, in the presence of different concentrations of free competing compound or vehicle (DMSO). pIC_{50} values are plotted against the pIC_{50} in the foci inhibition assay for each of the 11 compounds tested (dinaciclib, GW780056, SNS-032, AT7519, 488, 732, AG-12275, PD0332991, 155, GW805758, GW781673). r: Pearson correlation coefficient.

Fig. 5. CDK12 in DM1

(**A**) Western blot of protein from vastus lateralis muscle biopsy samples in non-DM1 and DM1 patients for CDK12. Blots are normalized to α-tubulin. (**B)** Histogram to quantify amounts of CDK12 protein normalized to α-tubulin (two tailed t-test, p=0.02, *N=4*). (**C)** Quantification of the number of CDK12 nuclear granules in DM1 and non-DM1 fibroblast cells (two tailed t-test, p<0.0001). (**D**) CDK12 protein granules (green) and CUG repeat expansion RNA foci (red) following shRNA treatment with scrambled control and CDK12 specific shRNAs**.** White bars=10μm **(E**) CDK12 granule number following shRNA treatment (two tailed t-test, p<0.0001) (**F**) CUG repeat expansion foci number following CDK12 shRNA treatment (two tailed t-test p<0.0001) Bars show mean ± SD. (**G**) CUG repeat expansion foci number following

overexpression of CDK12 full length open reading frame clone. (One way ANOVA, p=0.0017, *N=6*) (**H)** Experimental design for the inducible bi-directional plasmid expression 960 CTG repeats (**I**) Ethidium bromide stained gel showing CUG repeat RNA and eGFP RNA in the presence or absence of THZ531 inhibitor (**J**) ddPCR quantitative analysis showing transcription of 960 CUG repeat RNA and eGFP RNA with and without THZ531 treatment, normalized to endogenous GAPDH (2 way ANOVA: Sidak post-hoc: CUG 960 transcript -/+ THZ531, p=0.0038; eGFP transcript -/+ THZ531: ns) (**K**) Ethidium bromide stained gel showing CUG repeat RNA and eGFP RNA in the presence or absence of THZ531 inhibitor 24hrs after the removal of doxycycline following induction for 24hrs. (**L**) ddPCR quantitative analysis quantifying both CUG 960 and eGFP transcripts following removal of doxycycline, in the presence or absence of THZ531, compared to +DOX samples (normalized to endogenous GAPDH) Corresponding statistical values listed in Suppl. Dataset S3. (**M**) Nuclear run-on experiment in DM1 fibroblast cells quantifying wild type and mutant DMPK transcripts following CDK12 inhibition by THZ531 (two tailed t-test on mutant transcript, p=0.0017, *N=4*)

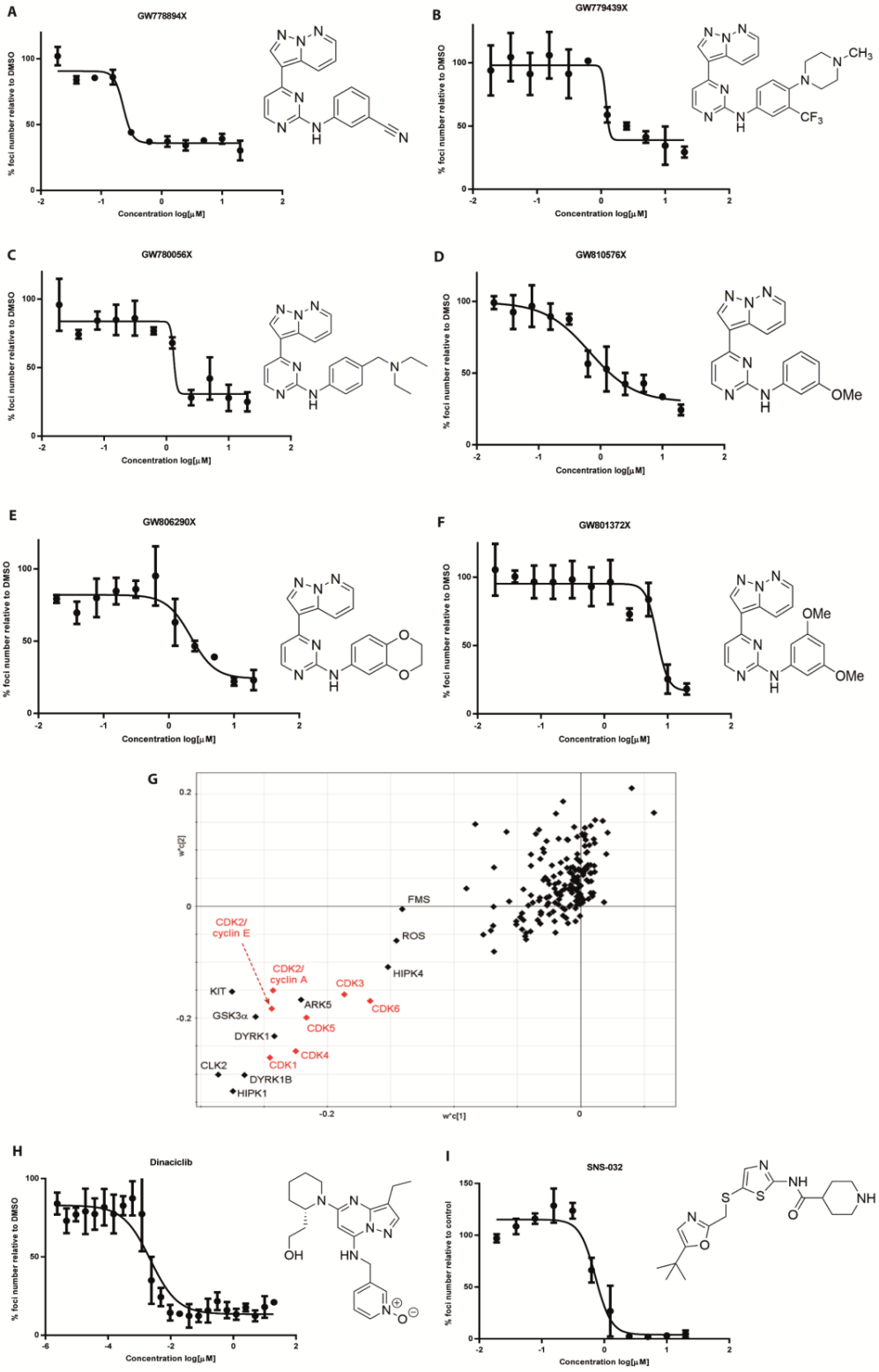
A
GW778894X
% foci number relative to DMSO
Concentration log[µM]
B
GW779439X
% foci number relative to DMSO
Concentration log[µM]
C
GW780056X
% foci number relative to DMSO
Concentration log[µM]
D
GW810576X
% foci number relative to DMSO
Concentration log[µM]
E
GW806290X
% foci number relative to DMSO
Concentration log[µM]
F
GW801372X
% foci number relative to DMSO
Concentration log[µM]
G
w*c[2]
w*c[1]
FMS
ROS
HIPK4
CDK2/
cyclin E
CDK2/
cyclin A
CDK3
CDK6
KIT
ARK5
GSK3α
CDK5
DYRK1
CDK4
CDK1
CLK2
DYRK1B
HIPK1
H
Dinaciclib
% foci number relative to DMSO
Concentration log[µM]
I
SNS-032
% foci number relative to control
Concentration log[µM]

Figure 1

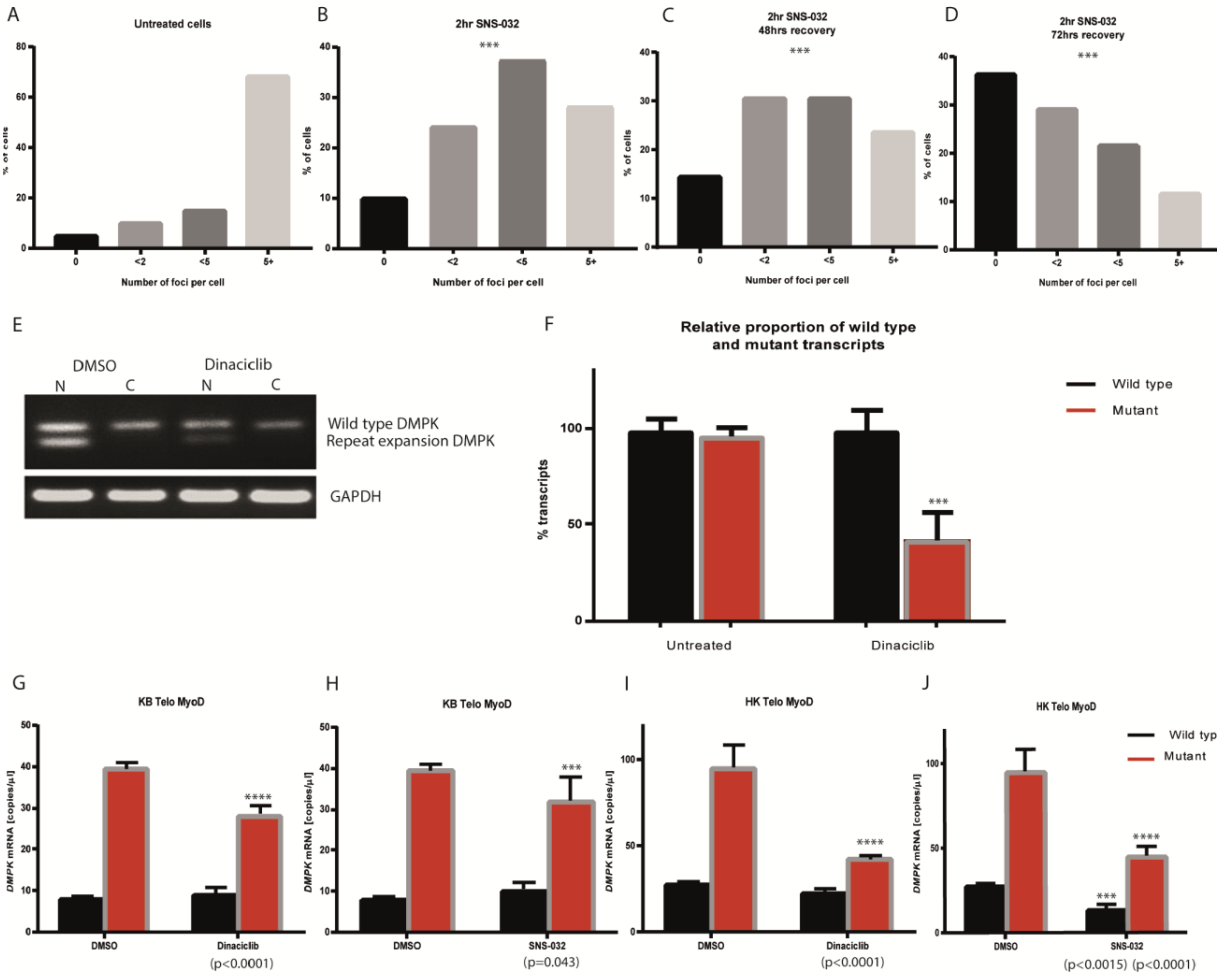
A
Untreated cells
% of cells
Number of foci per cell
B
2hr SNS-032
***
% of cells
Number of foci per cell
C
2hr SNS-032
48hrs recovery
***
% of cells
Number of foci per cell
D
2hr SNS-032
72hrs recovery
***
% of cells
Number of foci per cell
E
DMSO
Dinaciclib
N
C
N
C
Wild type DMPK
Repeat expansion DMPK
GAPDH
F
Relative proportion of wild type
and mutant transcripts
Wild type
Mutant
% transcripts
***
Untreated
Dinaciclib
G
KB Telo MyoD
DMPK mRNA [copies/µl]
****
DMSO
Dinaciclib
(p<0.0001)
H
KB Telo MyoD
DMPK mRNA [copies/µl]
***
DMSO
SNS-032
(p=0.043)
I
HK Telo MyoD
DMPK mRNA [copies/µl]
****
DMSO
Dinaciclib
(p<0.0001)
J
HK Telo MyoD
Wild typ
Mutant
DMPK mRNA [copies/µl]
***
****
DMSO
SNS-032
(p<0.0015) (p<0.0001)

Figure 2

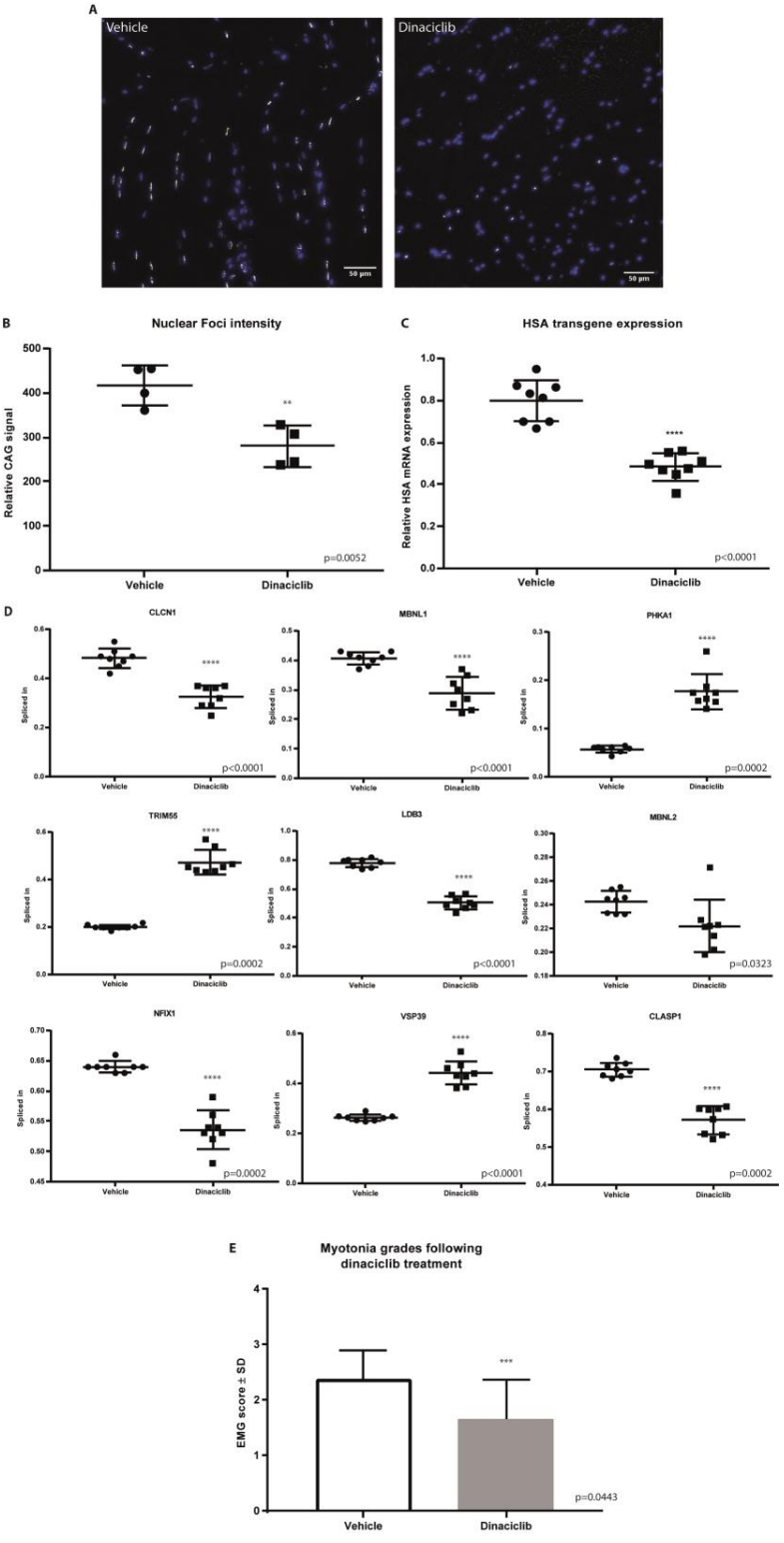
A
Vehicle
Dinaciclib
50 µm
B
Nuclear Foci intensity
Relative CAG signal
p=0.0052
Vehicle
Dinaciclib
C
HSA transgene expression
Relative HSA mRNA expression
p<0.0001
D
CLCN1
MBNL1
PHKA1
TRIM55
LDB3
MBNL2
NFIX1
VSP39
CLASP1
Spliced in
p<0.0001
p=0.0002
p=0.0323
E
Myotonia grades following dinaciclib treatment
EMG score ± SD
p=0.0443

Figure 3

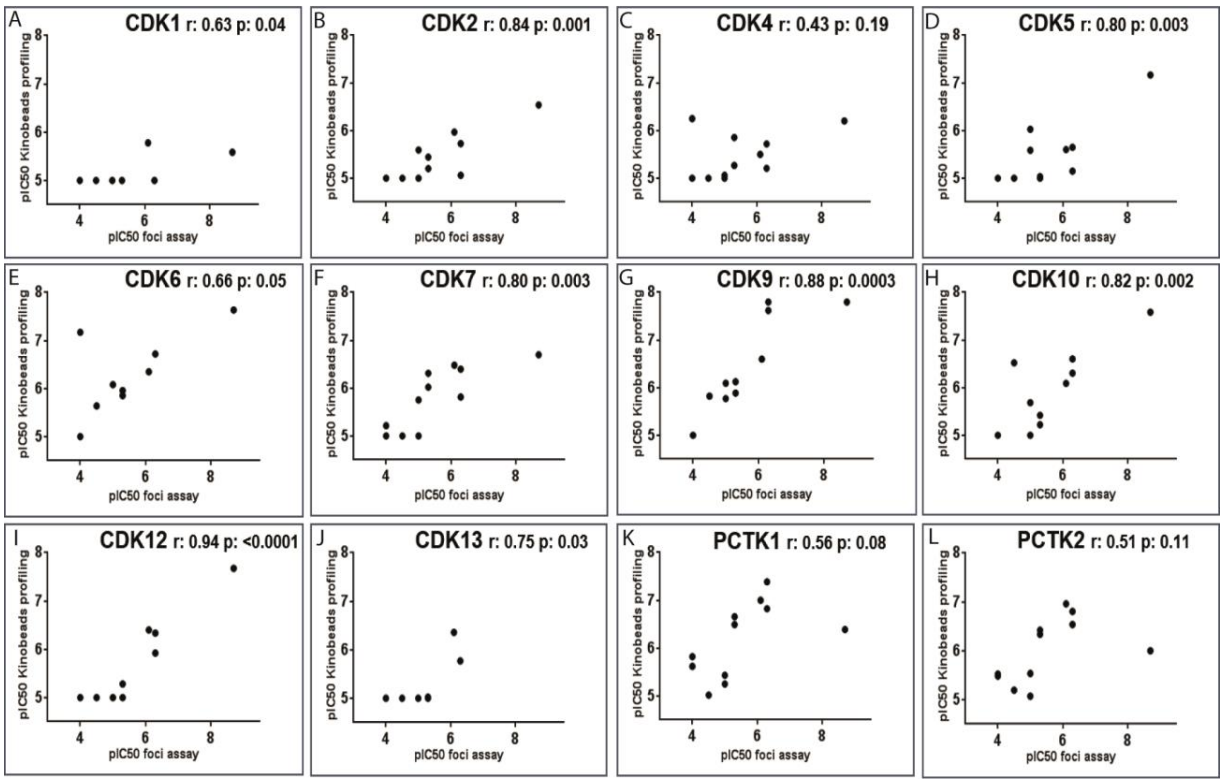
A
CDK1 r: 0.63 p: 0.04
B
CDK2 r: 0.84 p: 0.001
C
CDK4 r: 0.43 p: 0.19
D
CDK5 r: 0.80 p: 0.003
E
CDK6 r: 0.66 p: 0.05
F
CDK7 r: 0.80 p: 0.003
G
CDK9 r: 0.88 p: 0.0003
H
CDK10 r: 0.82 p: 0.002
I
CDK12 r: 0.94 p: <0.0001
J
CDK13 r: 0.75 p: 0.03
K
PCTK1 r: 0.56 p: 0.08
L
PCTK2 r: 0.51 p: 0.11
pIC50 Kinobeads profiling
pIC50 foci assay

Figure 4

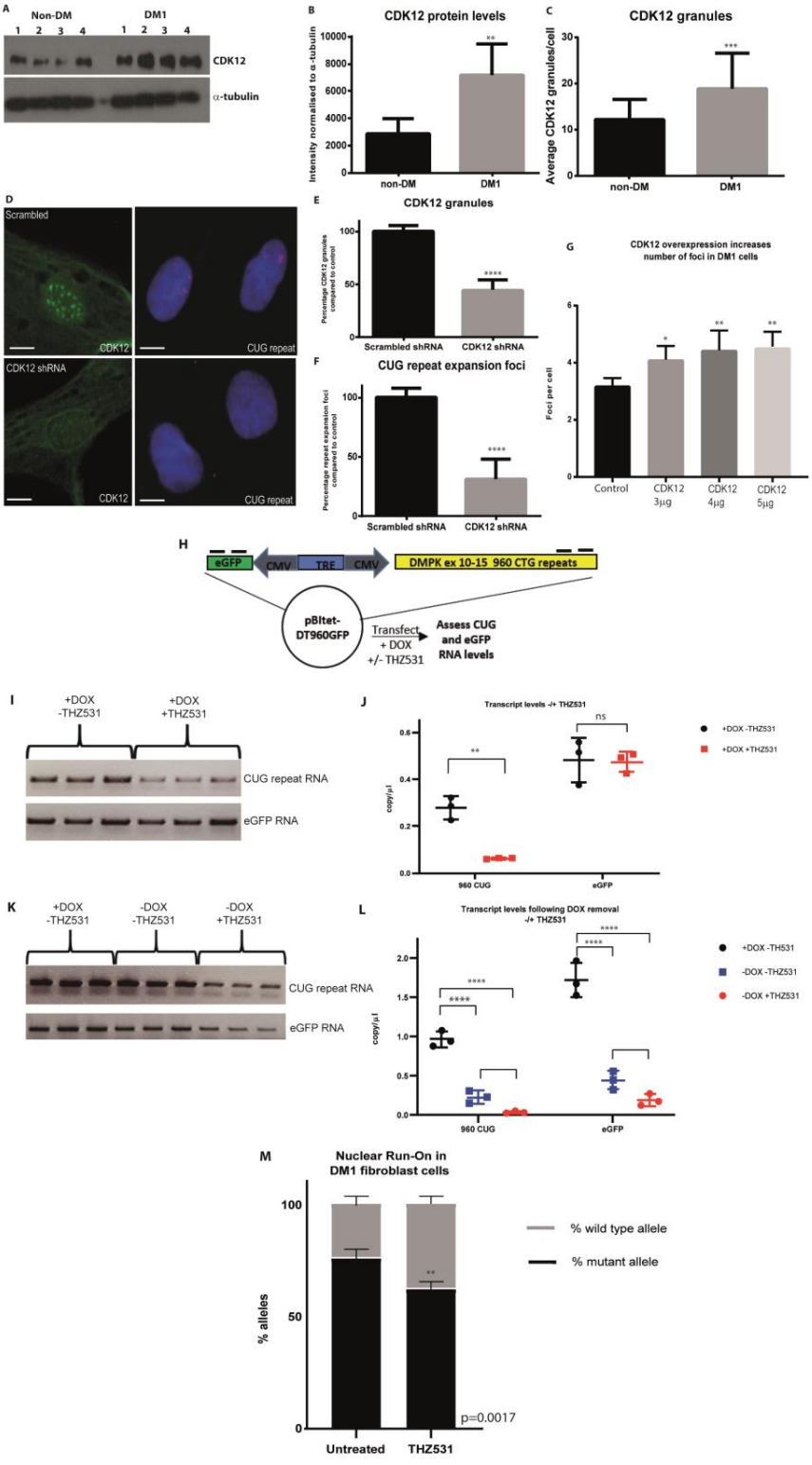
A
Non-DM
DM1
1 2 3 4 1 2 3 4
CDK12
α-tubulin
B
CDK12 protein levels
Intensity normalised to α-tubulin
non-DM
DM1
C
CDK12 granules
Average CDK12 granules/cell
non-DM
DM1
D
Scrambled
CDK12
CUG repeat
CDK12 shRNA
CDK12
CUG repeat
E
CDK12 granules
Percentage CDK12 granules compared to control
Scrambled shRNA
CDK12 shRNA
F
CUG repeat expansion foci
Percentage repeat expansion foci compared to control
Scrambled shRNA
CDK12 shRNA
G
CDK12 overexpression increases number of foci in DM1 cells
Foci per cell
Control
CDK12 3μg
CDK12 4μg
CDK12 5μg
H
eGFP
CMV
TRE
CMV
DMPK ex 10-15 960 CTG repeats
pBItet-DT960GFP
Transfect
+ DOX
+/- THZ531
Assess CUG and eGFP RNA levels
I
+DOX -THZ531
+DOX +THZ531
CUG repeat RNA
eGFP RNA
J
Transcript levels -/+ THZ531
copy/μl
960 CUG
eGFP
ns
+DOX -THZ531
+DOX +THZ531
K
+DOX -THZ531
-DOX -THZ531
-DOX +THZ531
CUG repeat RNA
eGFP RNA
L
Transcript levels following DOX removal -/+ THZ531
copy/μl
960 CUG
eGFP
+DOX -TH531
-DOX -THZ531
-DOX +THZ531
M
Nuclear Run-On in DM1 fibroblast cells
% alleles
% wild type allele
% mutant allele
p=0.0017
Untreated
THZ531

Figure 5

Supplementary Methods

Peptide and protein identification and quantification

Sample preparation and labeling with tandem mass tag (TMT) isobaric mass tags was performed essentially as described (*53*). For mass spectrometric analyses samples were dried in vacuo and resuspended in 0.1% formic acid in water and aliquots of the sample were injected into a nano-liquid chromatography (nano-LC) system coupled to a mass spectrometer: Eksigent 1D+ coupled to LTQ-OrbitrapXL mass spectrometer, Waters nanoAcquity coupled to Orbitrap Elite mass spectrometer, or Ultimate 3000 RSLC nano coupled to Q Exactive mass spectrometer (Thermo Fisher Scientific). Peptides were separated on custom 50 cm × 75 μM (internal diameter) reversed-phase columns (Reprosil) at 40 °C. Gradient elution was performed from 3% acetonitrile to 40% acetonitrile in 0.1% formic acid over 120–270min. LTQ-Orbitrap XL was operated with Xcalibur 2.0, Orbitrap Elite and Q Exactive instruments were operated with Xcalibur 2.2 software. Intact peptides were detected in the LTQ-OrbitrapXL/Orbitrap Elite at 30.000 resolution (measured at m/z = 400), in the Q Exactive at 70.000 resolution (m/z = 200). Internal calibration was performed with LTQ-OrbitrapXL using the ion signal from (Si(CH3)2O)6H+ at m/z 445.120025. Data-dependent tandem mass spectra were generated for up to ten peptide precursors (LTQ-OrbitrapXL/Orbitrap Elite six precursor, Q Exactive ten) using a combined collision-induced dissociation/higher-energy collisional dissociation (CID/HCD) (LTQ-Orbitrap XL) approach or using HCD only (Orbitrap Elite/Q Exactive) at a resolution of 15.000/17.500. For CID up to 5,000 ions (LTQ-Orbitrap XL) were accumulated in the ion trap (maximum ion accumulation time = 150 msec), for HCD up to 50.000 ions (LTQ-OrbitrapXL, maximum ion accumulation time = 350 msec), up to 30.000 ions (Orbitrap Elite, maximum ion accumulation time = 150 msec) and 1e6 ions (Q Exactive, maximum ion accumulation time = 60 msec) were accumulated in the HCD cell.

Mascot 2.3 and 2.4 (Matrix Science) was used for protein identification using 10 p.p.m. mass tolerance for peptide precursors and 0.6 Da (CID) or 20 mDa (HCD) tolerance for fragment ions. Carbamidomethylation of cysteine residues and TMT modification of lysine residues were set as fixed modifications and methionine oxidation, N-terminal acetylation of proteins and TMT modification of peptide N-termini were set as variable modifications. The search database consisted of a customized version of the International Protein Index database combined with a decoy version of this database created using a script supplied by Matrix Science. Criteria for protein quantification were: a minimum of 2 sequence assignments matching to unique peptides was required (false discovery rate (FDR) for quantified proteins <<0.1 %), Mascot ion score > 10, signal to background ratio of the precursor ion > 4, signal to interference > 0.5 (*56*). Reporter ion intensities were multiplied with the ion accumulation time yielding an area value proportional to the number of reporter ions present in the mass analyzer. Peptide fold changes were corrected for isotope purity as described and adjusted for interference caused by co-eluting nearly isobaric peaks as estimated by the signal-to-interference measure (*57*).

siRNA synthesis

The siRNA oligonucleotides were synthesized on an ABI 394 DNA/RNA synthesizer using a standard 0.2 μM scale protocol, but with a 10 min coupling time for each nucleotide addition step. Columns (SynBase^{TM} controlled pore glass (CPG) 1000Å, RNA: 0.2 μmol), standard 2'-O tert-butyldimethylsilyl (TBDMS) RNA-phosphoramidites and reagents for the synthesizer were purchased from Link Technologies Ltd., $MeNH_2$ solution (33 wt.% in ethanol) was obtained from Fluka, NEt_3•3HF, N-methylpyrrolidinone (NMP) were purchased from Aldrich, illustra Nap-10 columns were obtained from GE Healthcare Europe GmbH. Dichloromethane and acetonitrile were freshly distilled from CaH_2 before use on the synthesizer.

CDK12 siRNA knockdown

Scrambled: 5' ACGUGACACGUUCGGAGAAUU and CDK12: 5' CGAAAUAAUGAUGUUGGCACCAGUU siRNA sequences. Cells were electroporated on day 1 and day 4 with 800nM of scrambled or CDK12 siRNA using the Amaxa Nucleofector system. Cells were collected on day 7 for immunohistochemistry, in situ hybridisation and western blot analysis.

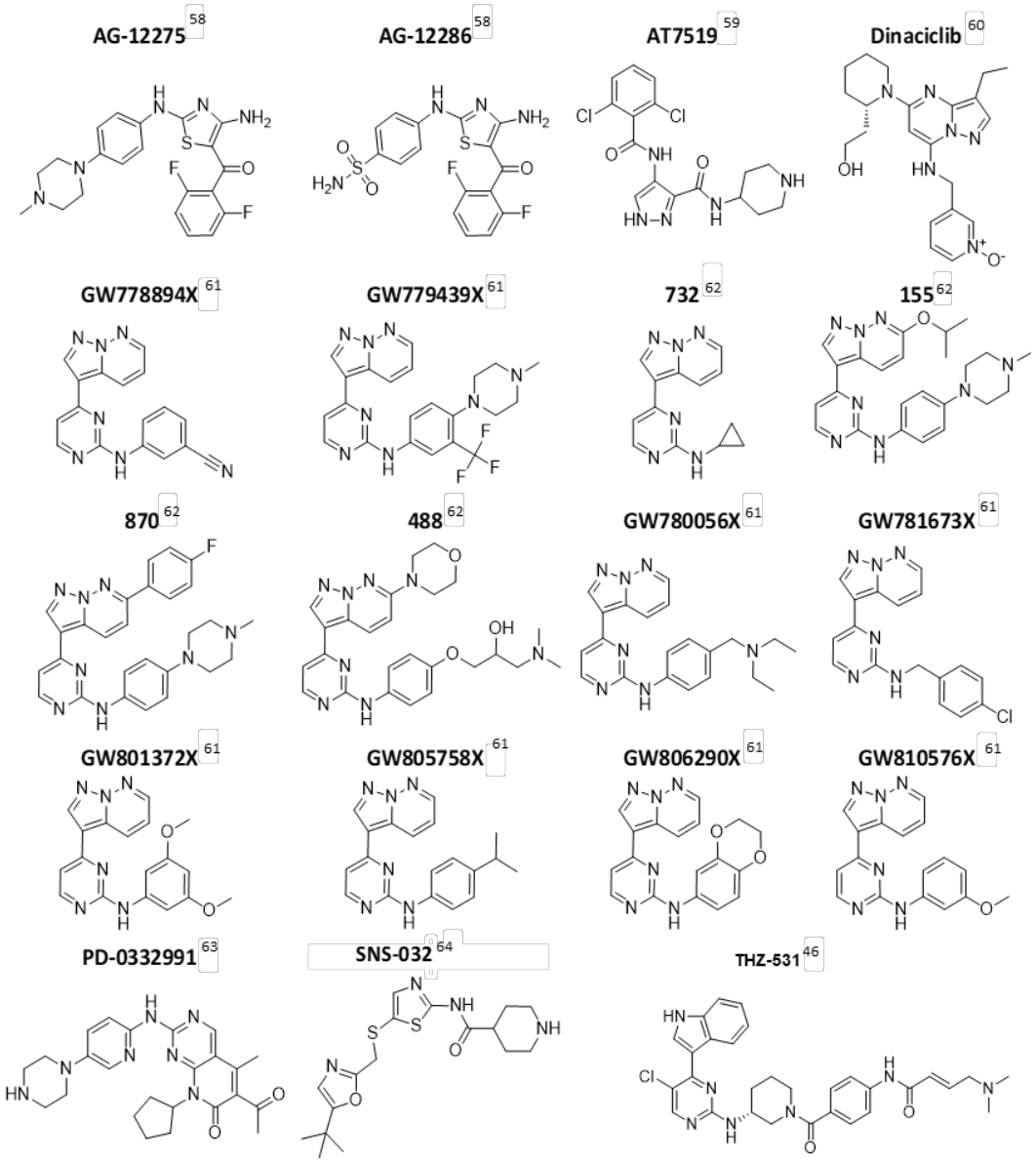

Fig. S1: Chemical structures of compounds used in this study

The chemical structures of all compounds used in the experiments of this study are shown above with references to the associated manuscripts for each compound.

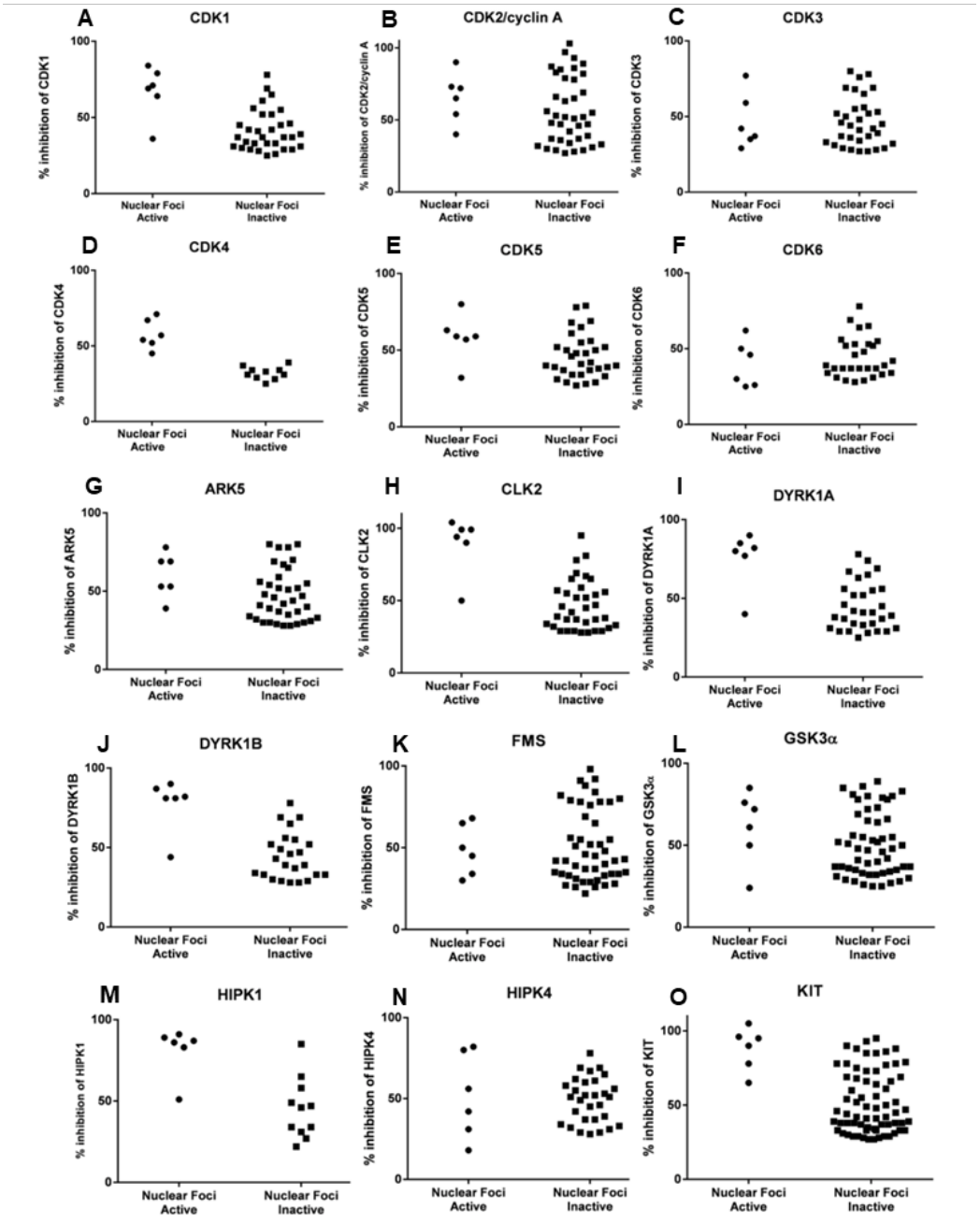

Fig. S2: Screening the PKIS collection identifies the CMGC kinase family

For each kinase target identified by the partial least squares analysis the percentage inhibition is plotted. (**A**) CDK1 (**B**) CDK2/cyclin A (**C**) CDK3 (**D**) CDK4 (**E**) CDK5 (**F**) CDK6 (**G**) ARK5

(**H**) CLK2 (**I**) DYRK1A (**J**) DYRK1B (**K**) FMS (**L**) GSK3α (**M**) HIPK1 (**N**) HIPK4 (**O**) KIT. The compounds are categorized into the six identified active nuclear foci reducing compounds and the remaining inactive compounds from the PKIS collection.

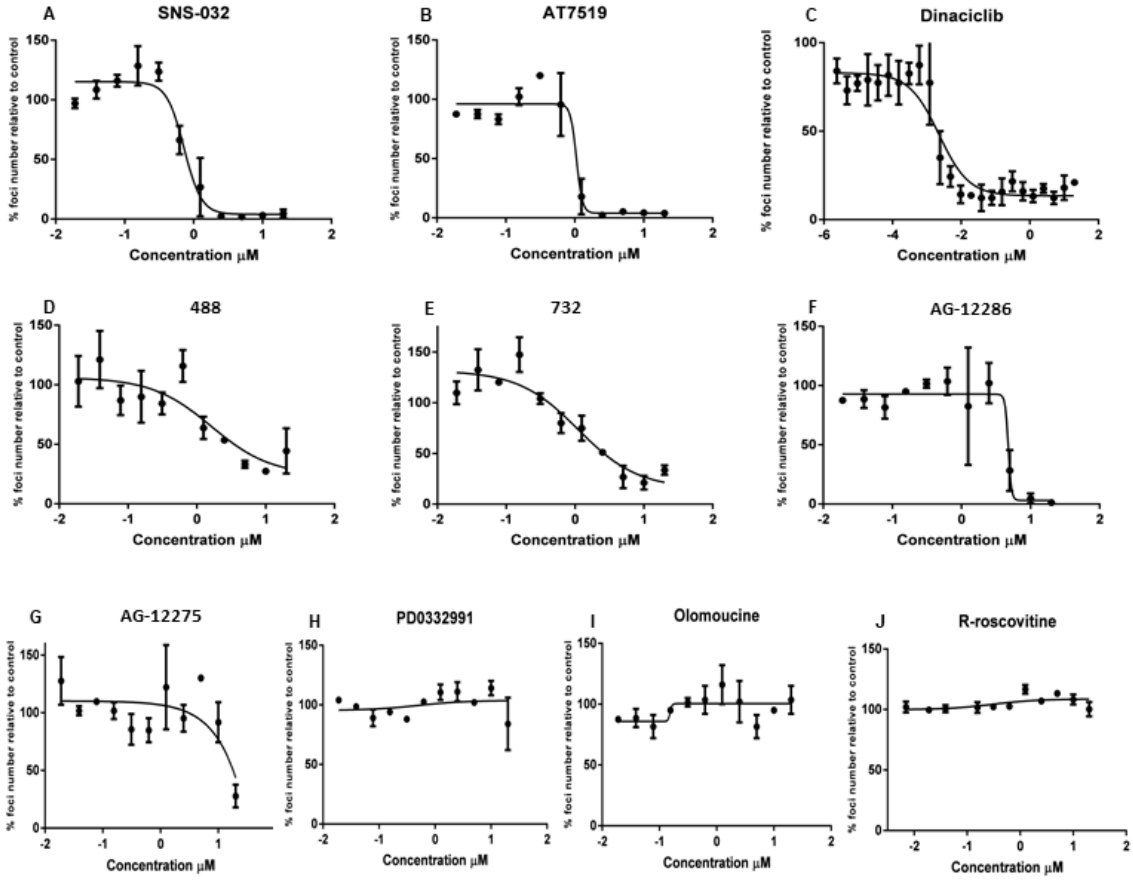

Fig. S3: CDK family inhibitor screen

Graphs show the percentage of nuclear foci relative to DMSO treated cells. DM1 fibroblast cells were treated with additional commercially available small molecule CDK inhibitors across adilution curve. (**A**) SNS-032 (**B**) AT7519 (**C**) Dinaciclib (**D**) 488 (**E**) 732 (**F**) AG-12286 (**G**) AG-12275 (**H**) PD0332991 (**I**) Olomoucine (**J**) R-roscovitine.

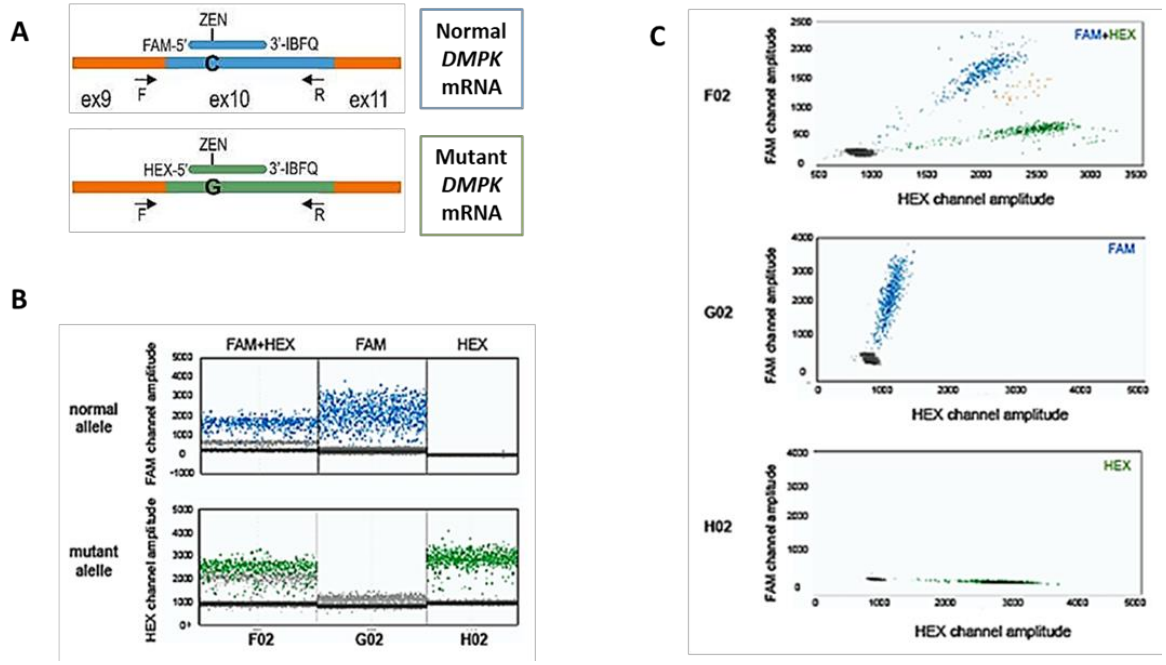

Fig. S4: Selectivity of the probes designed to recognize the SNP within *DMPK*

(**A**) Probe design: ZEN-Iowa Black dual-quencher probes used in *DMPK* copy number quantification in cDNA. The rs527221 SNP in exon 10 of *DMPK* (known as *Bpm*I polymorphism) was used to distinguish normal-size and mutant alleles. Position of primers (F and R) is shown by arrows and probes are displayed in their binding sites. For details about ddPCR probes and primers used in the analysis, please see Tables S5 and S6. (**B** and **C**) 1-D (panel B) and 2-D (panel C) amplitude plots: (**B**) 1-D amplitude plot of FAM- and HEX-labeled PCR products for normal and mutant *DMPK* mRNA in a human DM1 sample. FAM-positive and HEX-positive droplets are shown in blue and green, respectively, whereas negative droplets are shown in grey. (**C**) 2-D amplitude plot. Simultaneous utilization of two competitive probes (well F02). FAM-labelled probe only included in ddPCR reaction for the *Bpm*I SNP in exon 10 of *DMPK* (well G02). HEX-labelled probe only included in ddPCR reaction for the *Bpm*I SNP in exon 10 of *DMPK*. The

selectivity of the *Bpm*I SNP-recognizing probes was confirmed with alternative sets of probes with reversal of the fluorophores in their 5'-end (for more details, please see reference (33)).

Fig. S5: ddPCR used in aberrant splicing analysis

Probe design: An alternative exon inclusion probe (FAM-labeled) and alternative exon exclusion probe (HEX-labeled) used in alternative splicing assays; the probes have ZEN-Iowa Black as the dual-quencher. An alternative exon (exB) is indicated in red, and it's flanking exons (exA and exC) in blue and green. Location of primers (F and R) are shown by arrows and ZEN probes are displayed in their binding exons. For details about ddPCR probes and primers used in aberrant splicing analysis, please see Tables S5 and S6.

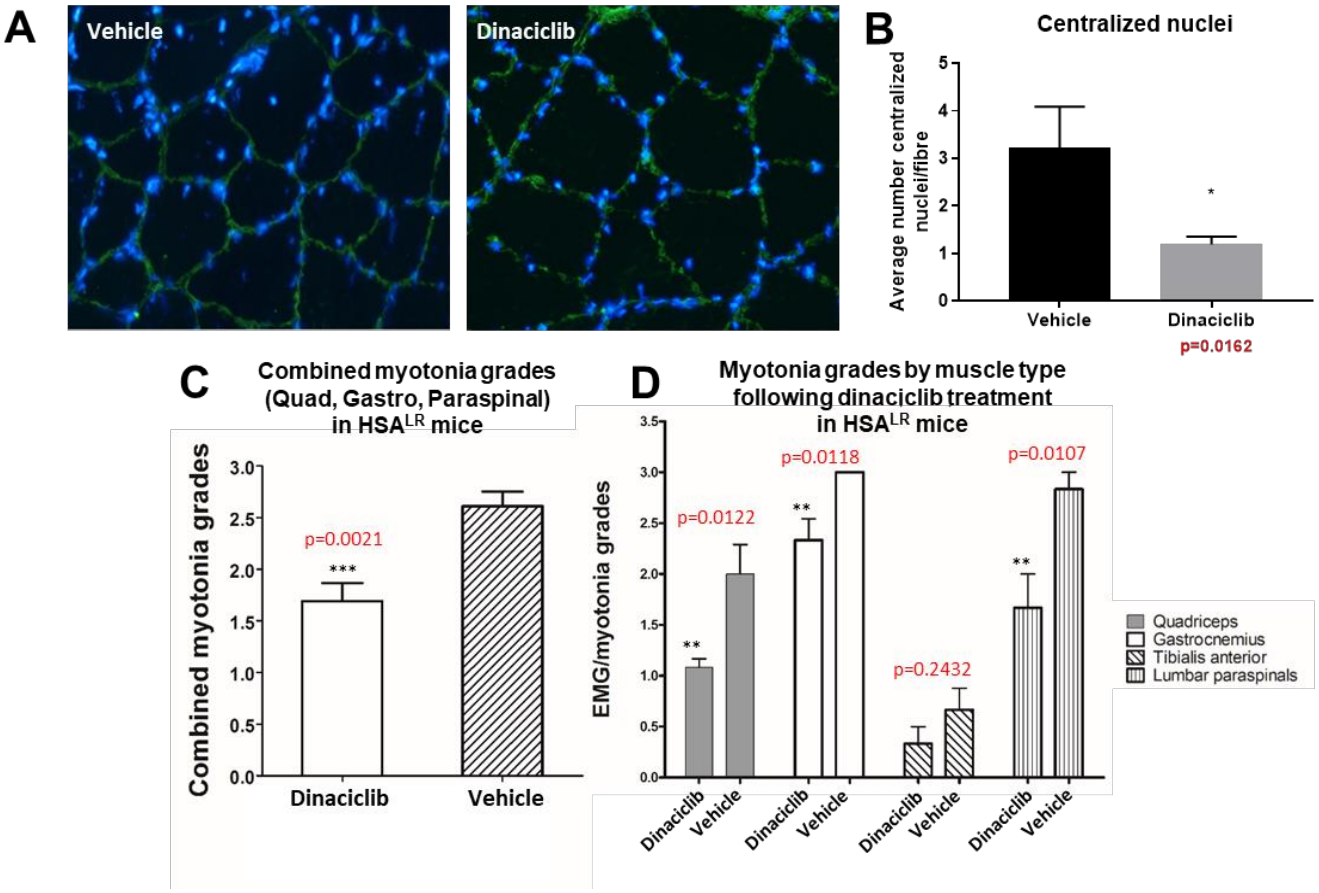

Fig. S6: HSA^{LR} muscle pathology and EMG analysis following dinaciclib treatment

(**A**) Laminin and hoescht stain to assess centralized nuclei in muscle fibres of vehicle control animals, compared to dinaciclib treated mice. (**B**) Average number of centralized nuclei per fibre in gastrocnemius muscle samples from vehicle and dinaciclib treated mice (t-test, p=0.0162). (**C**) Combined myotonia grade scores in quadriceps, gastrocnemius and paraspinal muscles from HSA^{LR} mice following vehicle and dinaciclib treatment (20mg/kg dose, 12 injections, mixed gender animals n=6 per treatment group, t-test p=0.0021). Myotonia was assessed by a blinded examiner and graded as follows: 0 indicates no myotonia; 1, occasional myotonic discharge in less than 50% of electrode insertions; 2, myotonic discharge in greater than 50% of insertions; 3, myotonic discharge with nearly every insertion. Wild type mice of the same inbred strain

background (FVB) do not show myotonia. (**D**) Myotonia grades by muscle type in dinaciclib and vehicle treated HSA^{LR} mice. (Bars show mean ±SD, p values calculated by t-tests)

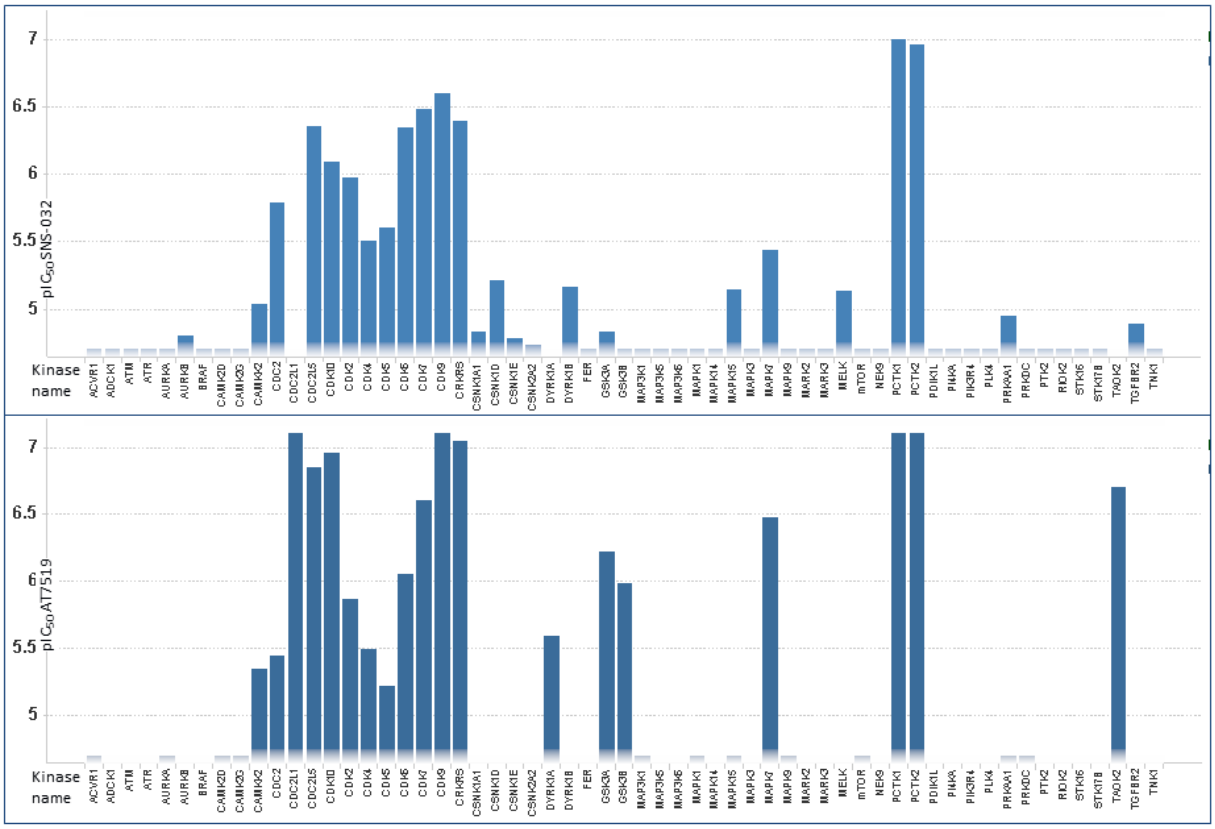

Fig. S7: Comparison of protein binding profiles for immobilized inhibitors SNS-032 and AT7519

Kinase selectivity profile of SNS-032 and AT7519: SNS-032 and AT7519 were immobilized to a bead-matrix and also used for competition. The figure shows all protein kinases affected by SNS-032 and AT7519 in a competition binding assay (no bar, protein was not identified; maximum compound concentration analyzed was 20 μM).

Name	Quant. unique peptides
CDC2	8
CDK2	8
CDK4	11
CDK5	6
CDK6	10
CDK7	8
CDK9	7
CDK10	2
CDK12	8
CDK13	10
PCTK1	8
PCTK2	3

CDC2 (CDK1)

MEDYTKIEKIGEGTYGVVYKGRHKTTGQVVAMKKKKIRLESEEEGVPSTAIREISLLKELRHPNIVSLQDVLMQDSRLYLIFEFLSMDLKKYLDSIPPGQ
YMDSSLVKVKAQSYLYQILQGIVFCHSRRVLHRDLKPQNLLIDDKGTIKLADFGLARAFGIPIRVYTHEVVTLWYRSPEVLLGSARYSTPVDIWSIGTIF
AELATKKPLFHGDSEIDQLFRIFRALGTPNNEVWPEVESLQDYKNTFPKWKPGSLASHVKNLDENGLDLLSKMLIYDPAKRISGKMALNHPYFNDLDNQI
KKM

CDK2

MENFQKVEKIGEGTYGVVYKARNKLTGEVVALKKIRLDTETEGVPSTAIREISLLKELNHPNIVKLLDVIHTENKLYLVFEFLHQDLKKFMDASALTGIP
LPLIKSYLFQLLQGLAFCHSHRVLHRDLKPQNLLINTEGAIKLADFGLARAFGVPVRTYTHEVVTLWYRAPEILLGCKYYSTAVDIWSLGCIFAEMVTRR
ALFPGDSEIDQLFRIFRTLGTPDEVVWPGVTSMPDYKPSFPKWARQDFSKVVPPLDEDGRSLLSQMLHYDPNKRISAKAALAHPFFQDVTKPVPHLRL

CDK4

MATSRYEPVAEIGVGAYGTVYKARDPHSGHFVALKSVRVPNGGGGGGGLPISTVREVALLRRLEAFEHPNVVRLMDVCATSRTDREIKVTLVFEHVDQDL
RTYLDKAPPPGLPAETIKDLMRQFLRGLDFLHANCIVHRDLKPENILVTSGGTVKLADFGLARIYSYQMALTPVVVTLWYRAPEVLLQSTYATPVDMWSV
GCIFAEMFRRKPLFCGNSEADQLGKIFDLIGLPPEDDWPRDVSLPRGAFPPRGPRPVQSVVPEMEESGAQLLLEMLTFNPHKRISAFRALQHSYLHKDEG
NPE

CDK5

MQKYEKLEKIGEGTYGTVFKAKNRETHEIVALKRVRLDDDDEGVPSSALREICLLKELKHKNIVRLHDVLHSDKKLTLVFEFCDQDLKKYFDSCNGDLDP
EIVKSFLFQLLKGLGFCHSRNVLHRDLKPQNLLINRNGELKLADFGLARAFGIPVRCYSAEVVTLWYRPPDVLFGAKLYSTSIDMWSAGCIFAELANAGR
PLFPGNDVDDQLKRIFRLLGTPTEEQWPSMTKLPDYKPYPMYPATTSLVNVVPKLNATGRDLLQNLLKCNPVQRISAEEALQHPYFSDFCPP

CDK6

MEKDGLCRADQQYECVAEIGEGAYGKVFKARDLKNGGRFVALKRVRVQTGEEGMPLSTIREVAVLRHLETFEHPNVVRLFDVCTVSRTDRETKLTLVFEH
VDQDLTTYLDKVPEPGVPTETIKDMMFQLLRGLDFLHSHRVVHRDLKPQNILVTSSGQIKLADFGLARIYSFQMALTSVVVTLWYRAPEVLLQSSYATPV
DLWSVGCIFAEMFRRKPLFRGSSDVDQLGKILDVIGLPGEEDWPRDVALPRQAFHSKSAQPIEKFVTDIDELGKDLLLKCLTFNPAKRISAYSALSHPYF
QDLERCKENLDSHLPPSQNTSELNTA

CDK7

MALDVKSRAKRYEKLDFLGEGQFATVYKARDKNTNQIVAIKKIKLGHRSEAKDGINRTALREIKLLQELSHPNIIGLLDAFGHKSNISLVFDFMETDLEV
IIKDNSLVLTPSHIKAYMLMTLQGLEYLHQHWILHRDLKPNNLLLDENGVLKLADFGLAKSFGSPNRAYTHQVVTRWYRAPELLFGARMYGVGVDMWAVG
CILAELLLRVPFLPGDSDLDQLTRIFETLGTPTEEQWPDMCSLPDYVTFKSFPGIPLHHIFSAAGDDLLDLIQGLFLFNPCARITATQALKMKYFSNRPG
PTPGCQLPRPNCPVETLKEQSNPALAIKRKRTEALEQGGLPKKLIF

CDK9

MQRDAPPRAPAPAPRLPAPPIGAAASSGGGGGGSGGGGGGASAAPAPPGLSGTTSPRGPGGGRRAEEAGSAPRGRKWPWRRKWRGRGGAWSAAAAGPGA
GAAAAATGGGGGALEAAMAKQYDSVECPFCDEVSKYEKLAKIGQGTFGEVFKARHRKTGQKVALKKVLMENEKEGFPITALREIKILQLLKHENVVNLIE
ICRTKASPYNRCKGSIYLVFDFCEHDLAGLLSNVLVKFTLSEIKRVMQMLLNGLYYIHRNKILHRDMKAANVLITRDGVLKLADFGLARAFSLAKNSQPN
RYTNRVVTLWYRPPELLLGERDYGPPIDLWGAGCIMAEMWTRSPIMQGNTEQHQLALISQLCGSITPEVWPNVDNYELYEKLELVKGQKRKVKDRLKAYV
RDPYALDLIDKLLVLDPAQRIDSDDALNHDFFWSDPMPSDLKGMLSTHLTSMFEYLAPPRRKGSQITQQSTNQSRNPATTNQTEFERVF

CDK10

MAEPDLECEQIRLKCIRKEGFFTVPPEHRLGRCRSVKEFEKLNRIGEGTYGIVYRARDTQTDEIVALKKVRMDKEKDGIPISSLREITLLLRLRHPNIVE
LKEVVVGNHLESIFLVMGYCEQDLASLLENMPTPFSEAQVKCIVLQVLRGLQYLHRNFIIHRDLKVSNLLMTDKGCVKTADFGLARAYGVPVKPMTPKVV
TLWYRAPELLLGTTTQTTSIDMWAVGCILAELLAHRPLLPGTSEIHQIDLIVQLLGTPSENIWPGFSKLPLVGQYSLRKQPYNNLKHKFPWLSEAGLRLL
HFLFMYDPKKRATAGDCLESSYFKEKPLPCEPELMPTFPHHRNKRAAPATSEGQSKRCKP

CDK12

MPNSERHGGKKDGSGGASGTLQPSSGGGSSNSRERHRLVSKHKRHKSKHSKDMGLVTPEAASLGTVIKPLVEYDDISSDSDTFSDDMAFKLDRRENDERRGSDRSD
RLHKHRHHQHRRSRDLLKAKQTEKEKSQEVSSKSGSMKDRISGSSKRSNEETDDYGKAQVAKSSSKESRSSKLHKEKTRKERELKSGHKDRSKSHRKRETPKSYKT
VDSPKRRSRSPHRKWSDSSKQDDSPSGASYGQDYDLSPSRSHTSSNYDSYKKSPGSTSRRQSVSPPYKEPSAYQSSTRSPSPYSRRQRSVSPYSRRRSSSYERSGS
YSGRSPSPYGRRRSSSPFLSKRSLSRSPLPSRKSMKSRSRSPAYSRHSSSHSKKKRSSSRSRHSSISPVRLPLNSSLGAELSRKKKERAAAAAAAKMDGKESKGSP
VFLPRKENSSVEAKDSGLESKKLPRSVKLEKSAPDTELVNVTHLNTEVKNSSDTGKVKLDENSEKHLVKDLKAQGTRDSKPIALKEEIVTPKETETSEKETPPPLP
TIASPPPPLPTTTPPPQTPPLPPLPPIPALPQQPPLPPSQPAFSQVPASSTSTLPPSTHSKTSAVSSQANSQPPVQVSVKTQVSVTAAIPHLKTSTLPPLPLPPLL
PGGDDMDSPKETLPSKPVKKEKEQRTRHLLTDLPLPPELPGGDLSPPDSPEPKAITPPQQPYKKRPKICCPRYGERRQTESDWGKRCVDKFDIIGIIGEGTYGQVY
KARDKDTGELVALKKVRLDNEKEGFPITAIREIKILRQLIHRSVVNMKEIVTDKQDALDFKKDKGAFYLVFEYMDHDLMGLLESGLVHFSEDHIKSFMKQLMEGLE
YCHKKNFLHRDIKCSNILLNNSGQIKLADFGLARLYNSEESRPYTNKVITLWYRPPELLLGEERYTPAIDVWSCGCILGELFTKKPIFQANLELAQLELISRLCGS
PCPAVWPDVIKLPYFNTMKPKKQYRRRLREEFSFIPSAALDLLDHMLTLDPSKRCTAEQTLQSDFLKDVELSKMAPPDLPHWQDCHELWSKKRRRQRQSGVVVEEP
PPSKTSRKETTSGTSTEPVKNSSPAPPQPAPGKVESGAGDAIGLADITQQLNQSELAVLLNLLQSQTDLSIPQMAQLLNIHSNPEMQQQLEALNQSISALTEATSQ
QQDSETMAPEESLKEAPSAPVILPSAEQMTLEASSTPADMQNILAVLLSQLMKTQEPAGSLEENNSDKNSGPQGPRRTPTMPQEEAAACPPHILPPEKRPPEPPGP
PPPPPPPPLVEGDLSSAPQELNPAVTAALLQLLSQPEAEPPGHLPHEHQALRPMEYSTRPRPNRTYGNTDGPETGFSAIDTDERNSGPALTESLVQTLVKNRTFSG
SLSHLGESSSYQGTGSVQFPGDQDLRFARVPLALHPVVGQPFLKAEGSSNSVVHAETKLQNYGELGPGTTGASSSGAGLHWGGPTQSSAYGKLYRGPTRVPPRGGR
GRGVPY

CDK13 (CDC2L5)

MPSSSDTALGGGGGLSWAEKKLEERRKRRRFLSPQQPPLLLPLLQPQLLQPPPPPPPLLFLAAPGTAAAAAAAAAASSSCFSPGPPLEVKRLARGKRRAGGRQKRR
RGPRAGQEAEKRRVFSLPQPQQDGGGGASSGGGVTPLVEYEDVSSQSEQGLLLGGASAATAATAAGGTGGSGGSPASSSGTQRRGEGSERRPRRDRRSSSGRSKER
HREHRRRDGQRGGSEASKSRSRHSHSGEERAEVAKSGSSSSSGGRRKSASATSSSSSSRKDRDSKAHRSRTKSSKEPPSAYKEPPKAYREDKTEPKAYRRRRSLSP
LGGRDDSPVSHRASQSLRSRKSPSPAGGGSSPYSRRLPRSPSPYSRRRSPSYSRHSSYERGGDVSPSPYSSSSWRRSRSPYSPVLRRSGKSRSRSPYSSRHSRSRS
RHRLSRSRSRHSSISPSTLTLKSSLAAELNKNKKARAAEAARAAEAAKAAEATKAAEAAAKAAKASNTSTPTKGNTETSASASQTNHVKDVKKIKIEHAPSPSSGG
TLKNDKAKTKPPLQVTKVENNLIVDKATKKAVIVGKESKSAATKEESVSLKEKTKPLTPSIGAKEKEQHVALVTSTLPPLPLPPMLPEDKEADSLRGNISVKAVKK
EVEKKLRCLLADLPLPPELPGGDDLSKSPEEKKTATQLHSKRRPKICGPRYGETKEKDIDWGKRCVDKFDIIGIIGEGTYGQVYKARDKDTGEMVALKKVRLDNEK
EGFPITAIREIKILRQLTHQSIINMKEIVTDKEDALDFKKDKGAFYLVFEYMDHDLMGLLESGLVHFNENHIKSFMRQLMEGLDYCHKKNFLHRDIKCSNILLNNR
GQIKLADFGLARLYSSEESRPYTNKVITLWYRPPELLLGEERYTPAIDVWSCGCILGELFTKKPIFQANQELAQLELISRICGSPCPAVWPDVIKLPYFNTMKPKK
QYRRKLREEFVFIPAAALDLFDYMLALDPSKRCTAEQALQCEFLRDVEPSKMPPPDLPLWQDCHELWSKKRRRQKQMGMTDDVSTIKAPRKDLSLGLDDSRTNTPQ
GVLPSSQLKSQGSSNVAPVKTGPGQHLNHSELAILLNLLQSKTSVNMADFVQVLNIKVNSETQQQLNKINLPAGILATGEKQTDPSTPQQESSKPLGGIQPSSQTI
QPKVETDAAQAAVQSAFAVLLTQLIKAQQSKQKDVLLEERENGSGHEASLQLRPPPEPSTPVSGQDDLIQHQDMRILELTPEPDRPRILPPDQRPPEPPEPPPVTE
EDLDYRTENQHVPTTSSSLTDPHAGVKAALLQLLAQHQPQDDPKREGGIDYQAGDTYVSTSDYKDNFGSSSFSSAPYVSNDGLGSSSAPPLERRSFIGNSDIQSLD
NYSTASSHSGGPPQPSAFSESFPSSVAGYGDIYLNAGPMLFSGDKDHRFEYSHGPIAVLANSSDPSTGPESTHPLPAKMHNYNYGGNLQENPSGPSLMHGQTWTSP
AQGPGYSQGYRGHISTSTGRGRGRGLPY

PCTK1

MQSEIAMDRMKKIKRQLSMTLRGGRGIDKTNGAPEQIGLDESGGGGGSDPGEAPTRAAPGELRSARGPLSSAPEIVHEDLKMGSDGESDQASATSSDEVQSPVRVR
MRNHPPRKISTEDINKRLSLPADIRLPEGYLEKLTLNSPIFDKPLSRRLRRVSLSEIGFGKLETYIKLDKLGEGTYATVYKGKSKLTDNLVALKEIRLEHEEGAPC
TAIREVSLLKDLKHANIVTLHDIIHTEKSLTLVFEYLDKDLKQYLDDCGNIINMHNVKLFLFQLLRGLAYCHRQKVLHRDLKPQNLLINERGELKLADFGLARAKS
IPTKTYSNEVVTLWYRPPDILLGSTDYSTQIDMWGVGCIFYEMATGRPLFPGSTVEEQLHFIFRILGTPTEETWPGILSNEEFKTYNYPKYRAEALLSHAPRLDSD
GADLLTKLLQFEGRNRISAEDAMKHPFFLSLGERIHKLPDTTSIFALKEIQLQKEASLRSSSMPDSGRPAFRVVDTEF

PCTK2

MKKFKRRLSLTLRGSQTIDESLSELAEQMTIEENSSKDNEPIVKNGRPPTSHSMHSFLHQYTGSFKKPPLRRPHSVIGGSLGSFMAMPRNGSRLDIVHENLKMGSD
GESDQASGTSSDEVQSPTGVCLRNRIHRRISMEDLNKRLSLPADIRIPDGYLEKLQINSPPFDQPMSRRSRRASLSEIGFGKMETYIKLEKLGEGTYATVYKGRSK
LTENLVALKEIRLEHEEGAPCTAIREVSLLKDLKHANIVTLHDIVHTDKSLTLVFEYLDKDLKQYMDDCGNIMSMHNVKLFLYQILRGLAYCHRRKVLHRDLKPQN
LLINEKGELKLADFGLARAKSVPTKTYSNEVVTLWYRPPDVLLGSSEYSTQIDMWGVGCIFFEMASGRPLFPGSTVEDELHLIFRLLGTPSQETWPGISSNEEFKN
YNFPKYKPQPLINHAPRLDSEGIELITKFLQYESKKRVSAEEAMKHVYFRSLGPRIHALPESVSIFSLKEIQLQKDPGFRNSSYPETGHGKNRRQSMLF

Fig. S8: CDK family member proteins identified by whole proteome analysis of DM1 fibroblasts

The table shows all CDK family members identified by whole proteome expression profiling of DM1 fibroblasts. To analyze the proteins in the extract by LC-MS/MS, a tryptic digest was performed. The identified peptides are indicated in red in the protein sequences.

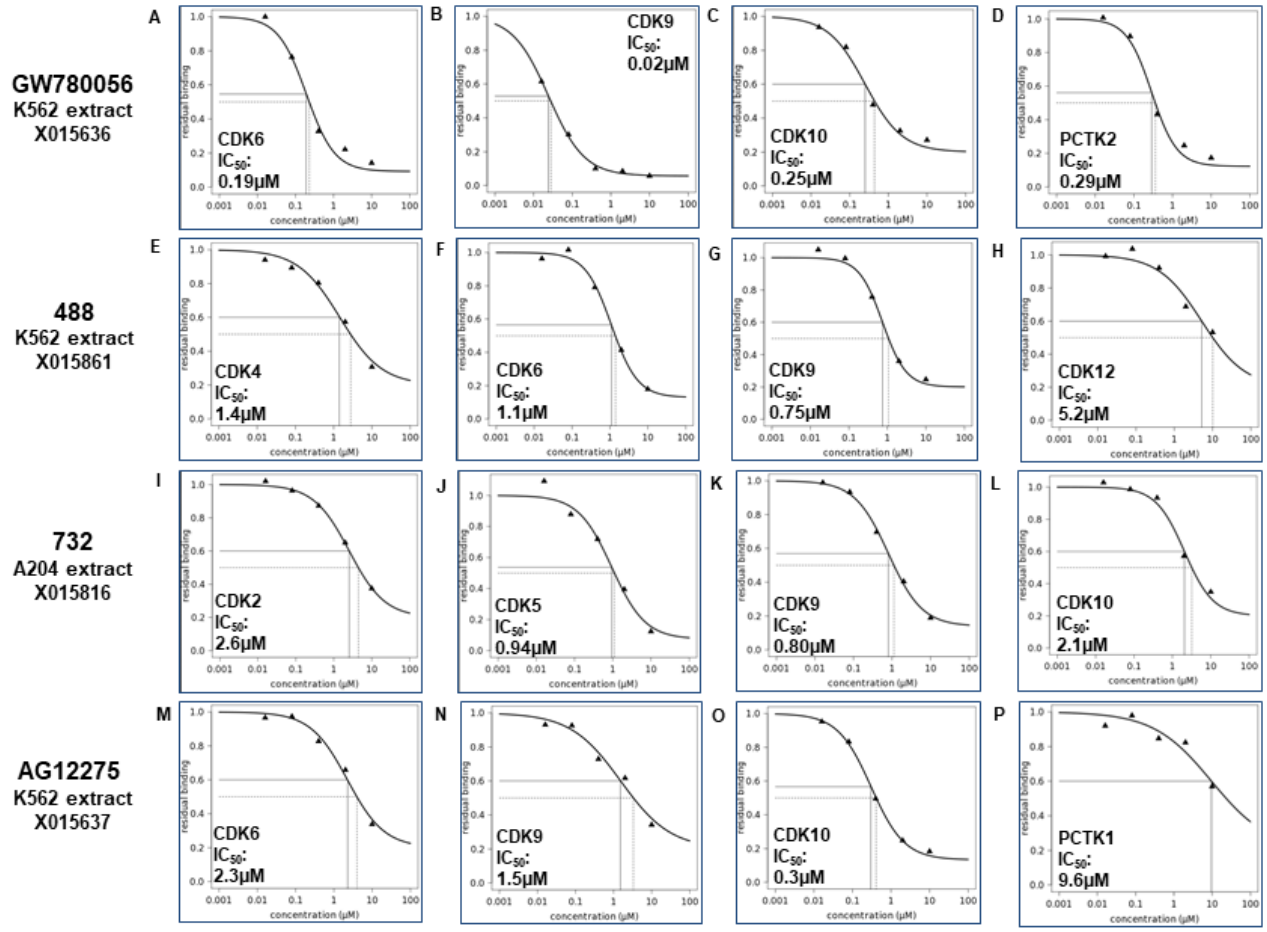

Fig. S9: Dose-response competition-binding curves for different compound/target combinations

An affinity matrix was generated by immobilization of SNS-032 to sepharose beads and affinity capturing was performed from (**A-H, M-P**) K562- or (**I-L**) A204 cell extract in the presence of vehicle (DMSO) or different concentrations of inhibitor as indicated. (**A-D**) GW780056 (**E-H**) 488 (**I-L**) 732 (**M-P**) AG12275. IC_{50} concentration and inflication points of the dose-response competition curves are indicated by dotted lines.

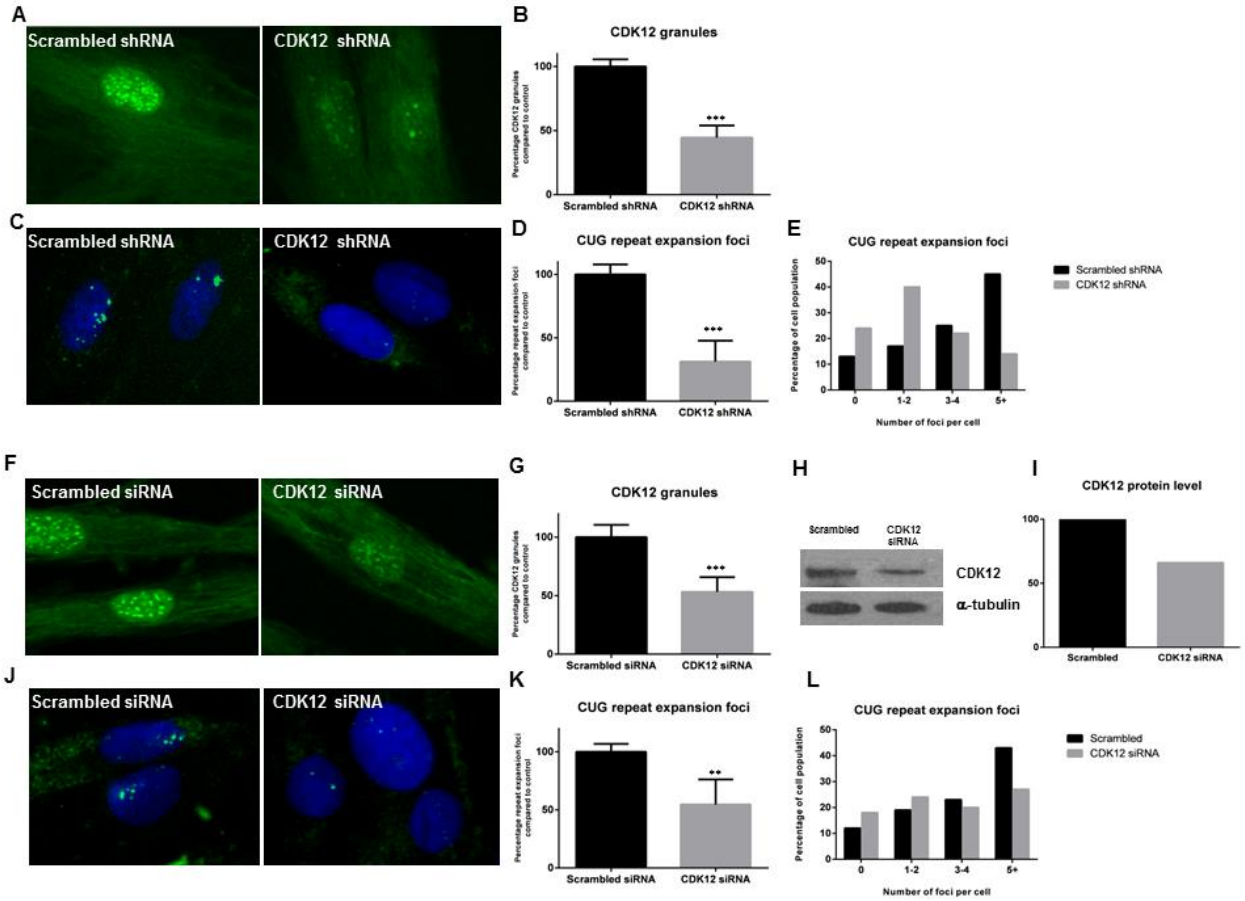

Fig. S10: CDK12 protein knockdown by siRNA and shRNA

(**A**) Immunohistochemistry of CDK12 with scrambled shRNA and CDK12-specific shRNA treatments. (**B**) Quantification of granule number with CDK12 shRNAs (t-test, $p<0.001$). (**C**) In situ hybridisation detecting nuclear foci following treatment with scrambled shRNA and CDK12-specific shRNA (**D**) Nuclear foci quantification following CDK12 shRNA treatment (t-test, $p<0.001$). (**E**) The distribution of cells containing 0-5+ foci were quantified for the cell population. **(F**) Immunohistochemistry of CDK12 with scrambled siRNA and CDK12-specific siRNA treatments. (**G**) Quantification of granule number with CDK12 siRNA (t-test, $p<0.001$). (**H-I**)

Western blot analysis shows the amount of CDK12 protein following CDK12 siRNA treatment. (**J**) In situ hybridisation detecting nuclear foci following treatment with scrambled siRNA and CDK12-specific siRNA. (**K**) Nuclear foci following CDK12 siRNA treatment (t-test, $p<0.01$). (**L**) The distribution of cells containing 0-5+ foci were quantified for the cell population.

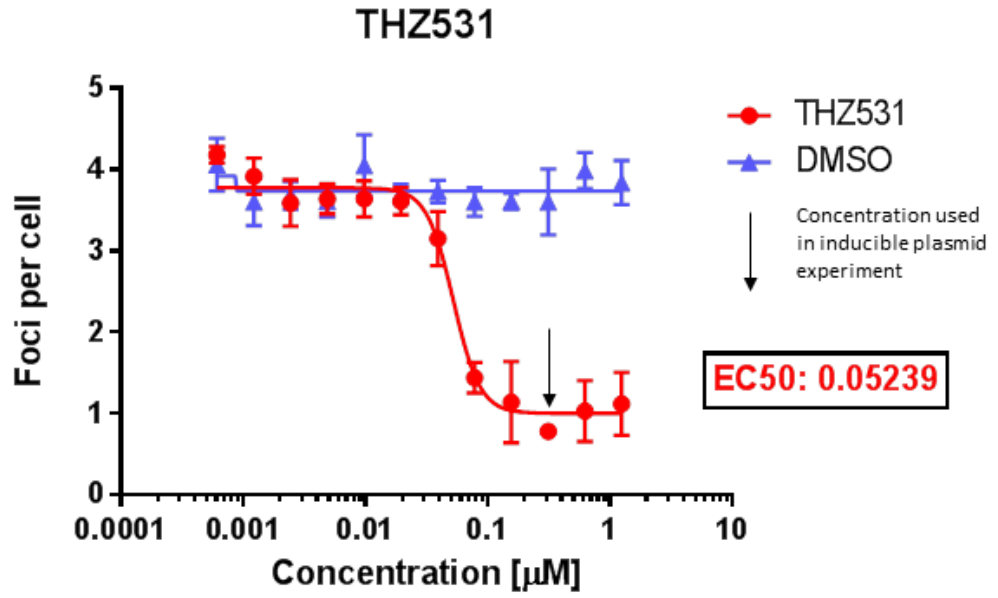

Fig. S11: THZ531 foci removal in DM1 fibroblast cells

12 point dilution of THZ531 in KB Telo MyoD cells compared to DMSO treatment.

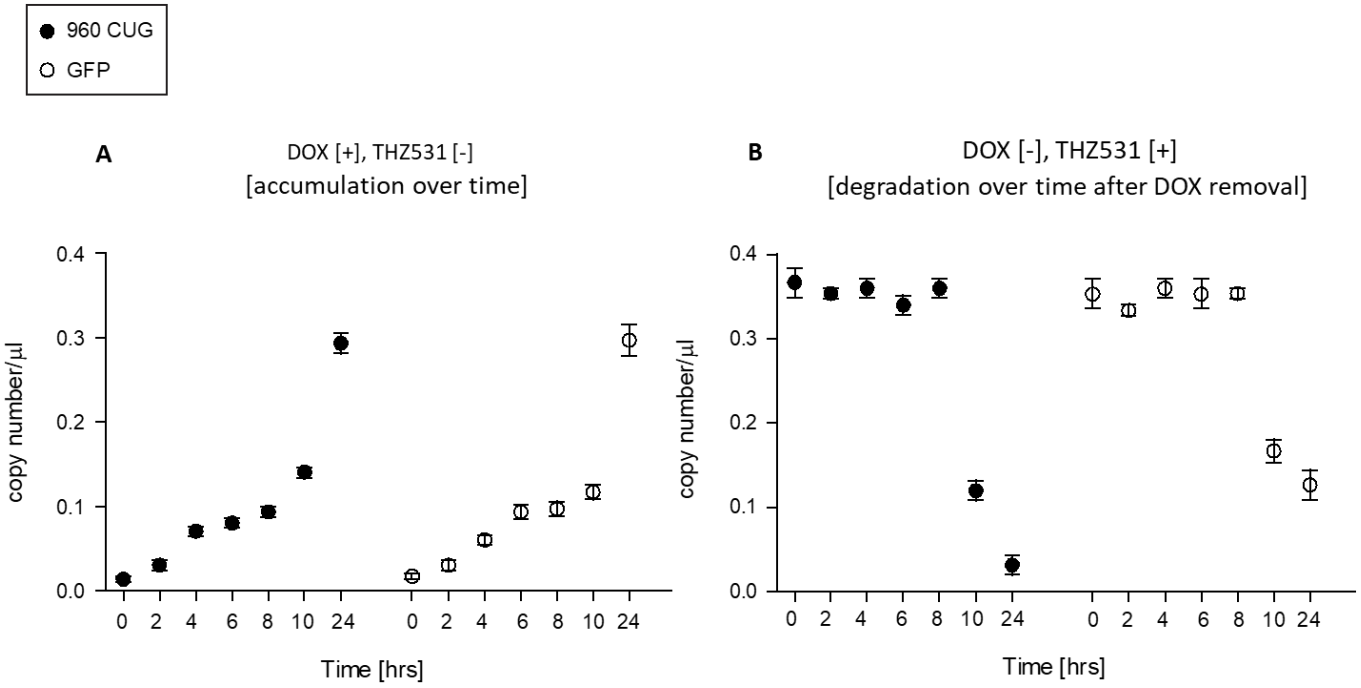

Fig. S12: Dynamics of the accumulation and degradation of CUG960 and eGFP transcripts

ddPCR analysis of RNA extracted from cells transfected with pBItet-DT960GFP shows the rate of accumulation and degradation (**A**) following induction with doxycycline (**B**) following removal of doxycycline.

	pIC50 value	
Compound	**KB Telo MyoD**	**LR Telo MyoD**
GW778894X	5.6	4.9
GW779439X	5.3	6.3
GW780056X	6.1	6.3
GW801372X	5.0	5.5
GW806290X	4.8	6.2
GW810576X	5.3	6.3

Table S1: pIC50 values in the nuclear foci assay of six PKIS hit compounds in two DM1 cell lines

	CDK1/ cyclin B	CDK2/ cyclin A	CDK3/ cyclin E	CDK4/ cyclinD3	CDK5/ p35	CDK6/ cyclin D3	CDK7/ cyclin H	CDK8/ cyclin C	CDK9/ cyclin T	Reference
Nuclear Foci Active										
Dinaciclib	72	2		127	45		170		178	65
AT7519	210	47	360	100	13	170	2400		<10	66
SNS-032 (BMS-387032)	480	38		925	340		62		4	67
488		450		38						62
AG-12275	325	220		3.3						68
AG-12286	2.2	5.7		13						68
732		120		80						62
Nuclear Foci Inactive										
PD0332991				9		15			400	69, 70
Olomoucine		7000			3000			94000	9100	71, 72
R-roscovitine	2690	700		1421	160		490			71, 73

Table. S2: IC50 values (nM) of previously reported CDK inhibitors

Compound Name	Dinaciclib	GW780056	SNS-032	AT7519	488	732	AG-12275	PD0332991	155	GW805758	GW781673
pIC50 foci assay	8.7	6.3	6.1	6	5.3	5	4.5	<4	<4	<4	<4
AAK1	1.05	0.17	0.95	0.96	0.09	0.45	0.97	0.76	0.1	0.84	0.89
ACVR1	0.99	0.37	0.97	0.97	0.32	0.84	0.98	1.05	0.72	0.94	1.03
AURKA	1.03	0.8	0.88	0.97	0.92	0.91	0.97	0.99	0.5	0.86	0.98
AURKB	0.99	0.27	0.89	0.98	0.92	0.75	0.94	0.82	0.79	1.02	0.98
BMP2K	1.05	0.28	0.96	0.98	0.14	0.81	1.01	0.79	0.16	0.92	0.92
CAMKK2	0.82	0.6	0.78	0.75	0.73	0.43	0.97	0.87	0.96	0.92	0.9
CDC2	0.54	0.51	0.39	0.39	0.78	0.61	0.9	0.92	0.89	0.93	0.87
CDK2	0.17	0.42	0.1	0.11	0.57	0.45	1.01	0.85	0.92	1.01	0.9
CDK5	0.19	0.7	0.6	0.37	0.87	0.56	1	0.88	0.94	0.92	0.84
CDK7	0.22	0.21	0.26	0.59	0.35	0.75	0.98	0.89	0.68	0.9	0.9
CDK9	0.11	0.14	0.16	0.16	0.3	0.2	0.64	0.64	0.86	0.51	0.41
CSNK1A1	0.96	0.2	0.81	0.99	0.67	0.52	0.95	1.02	0.99	0.9	0.73
CSNK1D	0.95	0.16	0.73	0.92	0.61	0.23	0.92	0.93	0.92	0.72	0.33
CSNK1E	0.9	0.33	0.89	1.07	0.71	0.44	1.07	0.99	0.92	0.82	0.67
CSNK2A1	0.99	0.46	0.96	0.96	0.31	0.61	0.9	0.58	0.46	0.68	0.95
CSNK2A2	1.02	0.24	0.9	0.93	0.08	0.54	1.02	0.24	0.11	0.67	0.98
GAK	1.01	0.59	0.92	0.98	0.19	0.87	1.05	0.98	0.31	1.04	1.01
GSK3A	0.95	0.6	0.34	0.09	0.99	1.01	1.03	1.14	1.07	0.86	1.1
GSK3B	0.96	0.66	0.55	0.21	1.07	1.03	0.93	1.09	1.12	0.86	1.06
IKBKE	1.07	0.99	1.02	1.06	0.83	0.95	1.03	1.01	0.5	0.91	0.99
JAK1	0.95	0.58	0.99	0.95	0.44	0.93	0.96	1.02	0.77	0.84	0.98
KIT	0.97	0.16	1	0.91	0.75	0.85	1.1	0.94	0.92	0.64	0.98
LIMK2	1.01	0.7	0.81	0.85	0.53	0.89	0.66	0.83	0.37	1.04	0.69
MAPK8	0.99	0.34	1.02	0.97	0.38	0.56	0.97	0.92	0.31	0.92	0.99
MAPK9	0.98	0.65	1.07	0.97	0.49	0.68	0.95	0.83	0.53	1.06	0.95
MELK	1.02	0.57	0.75	0.99	0.39	0.71	1	0.85	0.84	0.97	0.9
NEK9	1.02	0.42	1	1.01	0.26	0.79	1	1.08	0.06	0.86	1.02
PIK3C3	1.06	0.43	1	1.02	0.43	0.78	1.05	0.74	0.69	0.89	1.1
PIK3R4	0.96	0.5	1.01	1.05	0.5	0.84	0.93	0.65	0.72	0.89	0.97
PIP4K2A	0.85	0.62	0.95	0.93	0.63	0.82	0.9	0.45	0.95	0.73	0.73
PIP4K2C	0.96	0.22	0.96	0.98	0.36	0.75	1.04	0.21	0.83	0.64	0.8
PIP5K3	1	0.48	1.01	0.99	0.58	1	0.92	1.03	0.73	0.89	0.96
PTK2	1.02	0.33	0.95	0.98	0.7	0.95	0.96	0.98	0.92	0.92	0.95
RIOK2	0.98	0.49	0.91	1.01	0.43	0.53	1.03	1.07	0.94	0.77	0.77
STK16	0.9	0.33	1.14	1.15	0.35	0.98	1.08	0.48	0.41	0.92	1.14
TAOK2	0.9	0.86	0.84	0.32	0.75	0.66	0.9	0.82	0.7	1.03	0.94
TAOK3	0.69	0.77	0.96	0.45	0.82	0.78	0.95	0.8	0.67	0.93	1.05
TBK1	1.11	1.05	1.04	0.98	0.79	1.05	0.98	1.08	0.31	0.97	1
TYK2	0.95	0.4	0.93	0.91	0.46	0.93	0.91	0.95	0.84	0.92	0.9
ULK3	0.99	0.9	1.07	0.99	0.8	0.97	0.99	0.98	0.27	1.08	0.95

Table S3: Kinobeads profiling of a set of 11 compounds which represent a range of activities in the nuclear foci assay.

Target profiles were generated by adding each compound to K562 cell extract at a concentration of 2μM followed by incubation with Kinobeads and quantification of bead-bound proteins. Values indicate fold changes compared to vehicle control (loss of bead binding due to compound competition) Values highlighted in red show the strongest interacting kinase targets.

				pIC50 values from SNS-032 Kinobeads profiling in K562 and A204 extract												
Experiment identifier	Cell line	compound	pIC50 Foci assay	CDK1	CDK2	CDK4	CDK5	CDK6	CDK7	CDK9	CDK10	CDK12	CDC13	PCTK1	PCTK2
XO16768	K562	Dinaciclib	8.7	5.5	6.5	6.2	7.1	7.6	6.7	7.8	7.59	7.68		6.39	6
XO15636	K562	GW780056	6.3	<5	5.0	5.2	5.1	6.7	6.4	7.6	6.6	5.92	5.77	6.82	6.54
XO15785	A204	GW788056	6.3	<5	5.7	5.7	5.6		5.8	7.8	6.3	6.34		7.39	6.81
XO15510	K562	SNS-032	6.1	5.7	5.9	5.5	5.6	6.3	6.4	6.6	6.09	6.4	6.36	7	6.96
XO15861	K562	488	5.3	<5	5.4	5.8	5.0	5.9	6.3	6.1	5.42	5.28	5.02	6.66	6.42
XO15862	K562	488	5.3	<5	5.2	5.2	<5	5.8	6.0	5.8	5.22	<5	<5	6.49	6.34
XO15766	K562	732	5	<5	<5	5.0	5.5	6.0	<5	5.7	<5	<5	<5	5.25	5.07
XO15816	A204	732	5	<5	5.5	<5	6.0		5.7	6.0	5.69			5.43	5.53
XO15637	K562	AG-12275	4.5	<5	<5	<5	<5	6.6	<5	5.8	6.52	<5	<5	5.02	5.19
XO15706	K562	PD0332991	<4	<5	<5	6.2	<5	7.1	<5	<5	<5	<5	<5	5.82	5.52
XO15815	K562	155	<4	<5	<5	<5	<5	<5	5.2	<5	<5	<5	<5	5.62	5.48

Table S4: pIC50 values generated by affinity capturing with the SNS-032 affinity matrix in K562 cell extract for the different CDK inhibitors added to the cell extracts

Name	Alternative exon	Sequence
Clcn1_HEX	Ex7a	/5HEX/TGGTGTCTA/ZEN/TGAGCAGCCATAC/3IABkFQ/
Clcn1_FAM		/56-FAM/TGTCTATGA/ZEN/GGACCGTGCCTGG/3IABkFQ/
Nfix_HEX	Ex7	/5HEX/ACGTGGATG/ZEN/CAGGGAGCCCCCGG/3IABkFQ/
Nfix_FAM		/56-FAM/CGTGGATGC/ZEN/AGGCCCTGCTTCT/3IABkFQ/
Trim55_HEX	Ex9	/5HEX/TGGTGACAC/ZEN/AGATTGGATTTGA/3IABkFQ/
Trim55_FAM		/56-FAM/CTACCTCTC/ZEN/AGATTGGATTTGA/3IABkFQ/
MBNL1_HEX	Ex5	/5HEX/CAGCTGCCA/ZEN/TGGGAATTCCTCA/3IABkFQ/
MBNL1_FAM		/56-FAM/CAGCTGCCA/ZEN/TGACTCAGTCGGC/3IABkFQ/
Mbnl2_HEX	Ex7	/5HEX/CATCCCCAC/ZEN/AGATAATTCTGAA/3IABkFQ/
Mbnl2_FAM		/56-FAM/CCACAGTAC/ZEN/CCATGATGCACAG/3IABkFQ/
Vps39_HEX	Ex3	/5HEX/AAGGATGTT/ZEN/GGTTGTAACAGGTT/3IABkFQ/
Vps39_FAM		/56-FAM/TGAAAGCGG/ZEN/CAGTTGTAACAGGT/3IABkFQ/
PHKA1_HEX	E19	/5HEX/CAAGTAATG/ZEN/ATGTTCACATGTA/3IABkFQ/
PHKA1_FAM		/56-FAM/TGCATATAC/ZEN/AGAATGTTCACAT/3IABkFQ/
Clasp1_HEX	E23	/5HEX/ACGCTCTGA/ZEN/AGAAGCCTGTGAGA/3IABkFQ/
Clasp1_FAM		/56-FAM/CAGGAGCAA/ZEN/GAAGAAGCCTGTG/3IABkFQ/
Ldb3_HEX	Ex8	/5HEX/CGAAGGTCA/ZEN/AGGCCACAGGCCT/3IABkFQ/
Ldb3_FAM		/56-FAM/CGAAGGTCA/ZEN/AGCACCCCTATTG/3IABkFQ/
h_ACTA		/56-FAM/ATGCTTCTA/ZEN/GACACACTCCACCTCCA/3IABkFQ/
m_Gapdh		/5HEX/TGGAGAAAC/ZEN/CTGCCAAGTATGATGAC/3IABkFQ/
h_3'UTR DMPK (plasmid)		/56-FAM/AG GCC CTG A/ZEN/C GTG GAT GGG CAA /3IABkFQ/
EGFP (plasmid)		/5HEX/AC ATC GAG G/ZEN/A CGG CAG CGT GCA /3IABkFQ/
	***Bpm*I polymorphism**	
DMPK_HEX	G	5- /5HEX/CAC ACC CAT /ZEN/GGA A**G**T GGA GGC CGA GCA /3IABkFQ/ -3
DMPK_FAM	C	5- /56-FAM/CAC ACC CAT /ZEN/GGA A**C**T GGA GGC CGA GCA /3IABkFQ/ -3

Table S5: Dual-labeled probes used in ddPCR assays

Name	Alternative exon length [bp]	Sequence (5'-3')	PCR product length [bp]	Annealing temperature [°C]
Clcn1	79	**F:** TGGTAGCTTTGACAGCTGGACT	293	60
		R: GCACTCCTCCAAGTGGTGTT		
Nfix	123	**F:** CGACGACAGTGAGATGGAGAGT	296	60
		R: ACTGCTGGATGATGGACGTG		
Trim55	288	**F:** CTTCCCGCAGAGCTTCAGGT	468	54
		R: GCGAGCTGGCTCAGGATCA		
Mbnl1	54	**F:** GCCCAATACCAGGTCAACCA	160	60
		R: GAGCAGGCCTCTTTGGCAAT		
Mbnl2	95	**F:** GTCTTCAACCCCAGCGTCTT	346	54
		R: GAACTAGCCTTAGGGTTGTGGTCT		
Vps39	33	**F:** ACCAAGCAAGGGCATCTTCT	155	60
		R: ACCACATGGATCTGCTGGAT		
Phka1	177	**F:** GGCAACTGGATGGACAGCTA	321	54
		R: ATGAACGGAAGGAACCTGGC		
Clasp1	24	**F:** AGTACCAGCACTGACCTGGA	138	60
		R: GGAGGCATCACTGTTGGCAT		
Ldb3	186	**F:** GTCCTCCAACCTGCAGTCTC	352	54
		R: GTAGCTGGTATGGGCAGAGG		
ACTA	N/A	**F:** CCTTCCAGCAGATGTGGATCA	117	60
		R: TCGTCGTCCTGAGAAGTCG		
Gapdh	N/A	**F:**AAGGTCATCCCAGAGCTGAA	138	56
		R:CTGCTTCACCACCTTCTTGA		
EGFP_plasmid	N/A	**F:** TGAACTTCAAGATCCGCCACA	153	56
		R: TTCTCGTTGGGGTCTTTGCT		
3'UTR DMPK_plasmid	N/A	**F:** TTCTTTCTTTCGGCCAGGCT	127	56
		R: GCACTTTGCGAACCAACGAT		

Table S6: Primers used in ddPCR assays